

This is an Open Access document downloaded from ORCA, Cardiff University's institutional repository:<https://orca.cardiff.ac.uk/id/eprint/102849/>

This is the author's version of a work that was submitted to / accepted for publication.

Citation for final published version:

Anwer, M. Hafiz, Alves, Tiago MARcos , Aamir,, A. and Zubair 2017. Effects of sand-shale anisotropy on amplitude variation with angle (AVA) modelling: The Sawan Gas Field (Pakistan) as a key case-study for South Asia's sedimentary basins. *Journal of Asian Earth Sciences* 147 , pp. 516-531. 10.1016/j.jseaes.2017.07.047

Publishers page: <https://doi.org/10.1016/j.jseaes.2017.07.047>

Please note:

Changes made as a result of publishing processes such as copy-editing, formatting and page numbers may not be reflected in this version. For the definitive version of this publication, please refer to the published source. You are advised to consult the publisher's version if you wish to cite this paper.

This version is being made available in accordance with publisher policies. See <http://orca.cf.ac.uk/policies.html> for usage policies. Copyright and moral rights for publications made available in ORCA are retained by the copyright holders.



1 **Effects of sand-shale anisotropy on amplitude variation with angle (AVA)**  
2 **modelling: The Sawan Gas Field (Pakistan) as a key case-study for South**  
3 **Asia's sedimentary basins**

4 Hafiz Mubbasher Anwer<sup>1\*</sup>, Tiago M. Alves<sup>2</sup>, Aamir Ali<sup>1</sup>, Zubair<sup>3</sup>

5 <sup>1</sup>Department of Earth Sciences, Quaid-i-Azam University, Islamabad, 45320, Pakistan.

6 <sup>2</sup>3D Seismic Lab, School of Earth and Ocean Sciences, Cardiff University, Main Building-Park  
7 Place, Cardiff CF10 1JZ, United Kingdom

8 <sup>3</sup>Software Integrated Solutions, Schlumberger, Pakistan.

9 \* Corresponding author

10  
11 **Abstract**

12 Amplitude variation with angle (AVA) is a technique widely used in the characterisation of  
13 hydrocarbon reservoirs and assumes the Earth's crust to be an isotropic medium. Yet, seismic  
14 anisotropy is known to have first-order effects on seismic AVA responses when investigating  
15 subsurface prospects. This work analyses the effects of anisotropic strata on AVA responses  
16 using the Lower Goru Formation, middle Indus basin (Pakistan) as a case-study. In the study  
17 area, shale intervals are interbedded with reservoir sands of the Sawan gas field. Shales in this  
18 gas field form laminae or are dispersed within reservoir sands, making the Lower Goru  
19 Formation an example of a vertically transversely isotropic (VTI) medium. In this work, we  
20 calculate the effective (saturated) mechanical properties of the Lower Goru Formation based on  
21 rock physics templates; the Backus (1962) average typically designed for layered media,  
22 combined with the empirical relations of Brown and Korringa (1975) and Wood (1955). The  
23 input data used in our rock physics modelling is based on a detailed petrophysical analysis of  
24 well data. Using the saturated effective mechanical properties of the Lower Goru Formation, we

25 generate angle-dependent reflection coefficient curves (and seismic AVA responses) based on  
26 exact and approximate solutions, for both isotropic and anisotropic reservoir scenarios. Our  
27 results suggest that the effects of lithological anisotropy are more pronounced in places with  
28 thick shale beds within reservoir sands. Conversely, angle-dependent reflection curves, and  
29 seismic AVA responses based on isotropic or anisotropic cases, give similar solutions in the  
30 presence of thin shale beds. As a corollary of this work, we present a Bayesian inversion method  
31 for the estimation of porosity in VTI media.

32

33 **Keywords:** South Asia; VTI medium; Rüger's approximation; PP reflection coefficients;  
34 Anisotropic AVA Modelling; Bayesian inversion.

35

## 36 **1. Introduction**

37

38 Modern techniques based on the systematic analysis of amplitude variations of seismic  
39 waves with changing distance between source and receiver (AVO), or with angle of incidence  
40 (AVA), are widely used in the petroleum industry to: a) detect subsurface gas, b) identify  
41 lithological variations, and c) analyse subsurface fluid volumes and compositions (Floridia and  
42 Teles, 1998; Grechka, 1998; Margesson and Sondergeld, 1999; Feng and Bancroft, 2006;  
43 Almutlaq and Margrave, 2010; Chao et al., 2012). Seismic AVA is of particular interest as its  
44 use is based on the realisation that variations in amplitude, at varying incident angles, result from  
45 contrasts in lithology and fluid content in rocks above and below a layer boundary (Zhang and  
46 Brown, 2001). Seismic AVA modelling is systematically carried out in reservoir studies by  
47 considering the Earth as an isotropic medium. However, all sedimentary rocks exhibit anisotropic  
48 behaviour at different scales (Xu et al., 2005). It has been known for a long time that anisotropy  
49 resulting from shaley beds and lenses within sandy successions can affect seismic AVA  
50 responses when investigating sand-shale reservoirs (Banik, 1987; Wright, 1987; Kim et al., 1993;

51 Thomsen, 1995; Blangy, 1994; Ball, 1995; Grechka, 1998; Besheli et al., 2005; Brajanovski et  
52 al., 2009; Chao et al., 2012; Nourollah et al., 2015). By ignoring the effects of anisotropy during  
53 AVA modelling, interpreters may complete erroneous characterisations of productive reservoir  
54 intervals (Besheli et al., 2005). Importantly, erroneous quantification of volumes and reservoir  
55 distribution(s) should arise when analysing the petroleum potential of sedimentary basins in  
56 South Asia, and other parts of the world, where stratified reservoir sequences of shale and silt  
57 contain significant amounts of ‘tight oil’ and ‘tight gas’ (McGlade et al., 2012; Katz and Lin,  
58 2014; English et al., 2015; Rodriguez et al., 2016).

59 In recent decades, stratigraphic sequences of thin-layered sands and shales have become  
60 key exploration targets for which seismic anisotropy methods (also referred to as long-  
61 wavelength anisotropy) are useful and broadly successful in their characterisation (Crampin et  
62 al., 1984; Sayers, 2013; Sone and Zoback, 2013; Das and Zoback, 2013). Shale layers within a  
63 horizontally-bedded sand matrix behave elastically as transversely isotropic (TI) media, i.e. they  
64 have similar wave properties in two perpendicular directions, but are significantly different in a  
65 third orthogonal direction (Sone and Zoback, 2013). In these same sequences, vertical axes of  
66 symmetry are often described as vertically transversely isotropic (VTI) media (da Silva et al.,  
67 2016; Li et al., 2016).

68 The anisotropic behaviour of VTI media is usually quantified by using Thomsen's  
69 anisotropic parameters  $\epsilon$ ,  $\delta$ ,  $\gamma$  (Thomsen, 1986), in which  $\epsilon$  denotes the fractional difference  
70 between the horizontal and vertical P-wave velocities,  $\delta$  describes the variation in P-wave  
71 velocity with phase angle for near-vertical propagation, and  $\gamma$  denotes the fractional difference  
72 between the horizontal and vertical SH-wave velocity (Rüger, 2002). The empirical forms of  $\epsilon$ ,  
73  $\delta$ ,  $\gamma$  are provided by Rüger (2002) as:

74

$$75 \quad \gamma = \frac{C_{66} - C_{55}}{2C_{55}}, \quad (1)$$

76 
$$\varepsilon = \frac{C_{11} - C_{33}}{2C_{33}}, \quad (2)$$

77 and

78 
$$\delta = \frac{(C_{13} + C_{55})^2 - (C_{33} - C_{55})^2}{2C_{33}(C_{33} - C_{55})}. \quad (3)$$

79

80 Here,  $C$  represents the stiffness and its indices denote standard constants for VTI media. In  
 81 essence, elastic anisotropy in VTI media can be characterised by five independent elastic  
 82 constants, which can be expressed in two notations: a) in terms of stiffness constants  
 83 ( $C_{11}, C_{13}, C_{33}, C_{55}$  &  $C_{66}$ ), or b) in terms of vertical velocities ( $V_P$  and  $V_S$ ) and Thomsen's  
 84 anisotropic parameters ( $\varepsilon, \delta, \gamma$ ) (Tsvankin, 1997a, 1997b). These five independent elastic  
 85 constants are very difficult to apply to AVA analyses, and most of these latter are developed by  
 86 assuming a non-VTI medium.

87 Several researchers have attempted to estimate seismic anisotropy and incorporate it into  
 88 AVA-based methods using seismic, VSP, well logs and core data (Blangy, 1992, Leaney, 1993;  
 89 Blangy, 1994, Margesson and Sondergeld, 1999; Besheli et al., 2005, Luo et al., 2005, Wang et  
 90 al., 2006; Brajanovski et al., 2009; Goodway et al., 2010; Wang, 2011), but seldom for  
 91 hydrocarbon-rich basins in South Asia. However, in the Indian subcontinent (including Pakistan  
 92 and bordering countries), important tight oil and gas reservoirs have been found in the hinterland  
 93 basins that surround the Himalayan and Baluchistan mountain ranges. The Indus basin is  
 94 currently the main focus of oil and gas exploration and production in Pakistan (Alam et al., 2014;  
 95 Asim et al., 2015) (Figure 1a). In this basin, as in other hydrocarbon-productive regions of South  
 96 and Southeast Asia, the successful use of AVA techniques in reservoir characterisation is  
 97 critically dependent upon the careful estimation of the anisotropic parameters of sedimentary  
 98 rocks (Zaigham and Mallick, 2000; Chengzao et al., 2012; Zhu et al., 2012; Jinhu et al., 2014).

99 In this work, we use well log data from the Sawan gas field (Figure 1b), middle Indus basin  
100 (Pakistan), to focus on the Cretaceous Lower Goru C-sand reservoir, which is interbedded with  
101 shales. We use reservoir properties estimated from borehole data as key data inputs to our rock  
102 physics models, and to later carry out anisotropic and isotropic AVA analyses. Rock physics  
103 models are often used to link seismic data to reservoir properties (Avseth et al., 2005). Seismic-  
104 based estimates of reservoir properties can be uncertain, but the inclusion of rock physics models  
105 in exploration workflows is, nevertheless, capable of reducing the level of uncertainty by  
106 decreasing the number of unknown parameters in AVA analyses. In other words, rock physics  
107 modelling represents a type of regularization within the context of seismic inversion (Ali and  
108 Jakobsen, 2011a, 2011b).

109 The aim of this work is to analyse the effects of anisotropy generated by interbedded shales  
110 within the reservoir sands, and its implications to AVA-based reservoir studies. In parallel, we  
111 investigate how accurate are seismic AVA methods for both exact (Zoeppritz, 1919; Daley and  
112 Horn, 1977) and approximate (Rüger, 1998; 2002) solutions for PP-reflection coefficients within  
113 the context of isotropic and anisotropic cases.

114

## 115 **2. Geological setting**

116

117 The Sawan gas field lies in the middle Indus basin, in the eastern border of Pakistan (Zaigham  
118 and Mallick, 2000). The study area is bounded by the Sargodha High to the north, and by the  
119 Jacobabad and Mari-Kandkot Highs to the south (Figure 1a). The Indian Shield bounds the  
120 eastern side of the study area, whereas the Kirthar and Suleiman fold-and-thrust belts mark its  
121 western boundary (Kadri, 1995; Afzal et al., 2009). Regional geological data indicate that the  
122 structural evolution of the Sawan gas field was closely controlled by three post-rift tectonic  
123 events: a) Late Cretaceous uplift and erosion, b) NW-trending thick-skinned wrench faulting and  
124 c) Late Tertiary to present-day tectonic uplift of the Jacobabad and Khairpur Highs (Ahmad et

125 al., 2004; Afzal et al., 2009; Azeem et al., 2016). These latter structural highs played an important  
126 role in the formation of structural and stratigraphic traps, not only in the Sawan area, but also in  
127 multiple oil and gas fields in the region (Ahmad et al., 2004; Fink et al., 2004; Berger et al.,  
128 2009).

129 Cretaceous black shales in the Sembar Formation are the proven source rock in the middle  
130 and lower Indus basins, which were mainly filled with shale and minor amounts of black  
131 siltstone, sandstone and nodular argillaceous limestone (Quadri and Shuaib, 1986; Kadri, 1995).  
132 The thickness of the Sembar Formation ranges from 0 m to more than 260 m (Iqbal and Shah,  
133 1980). The Sembar Formation is deeply buried and matures thermally towards the western edge  
134 of the Indus basin. It becomes shallower and less mature towards its eastern edge (Wandrey et  
135 al., 2004). In the study area, the tectonic uplift recorded by the Khairpur High controlled the  
136 depositional patterns of the main reservoir unit (Goru Formation); reservoir sands in proximal  
137 depositional systems are positioned in structurally deep areas, whereas non-reservoir distal shales  
138 are positioned up-dip to form major structural traps (Azeem et al., 2016, Berger et al., 2009). The  
139 depositional environment of the Lower Goru Member, which comprises the main reservoir  
140 interval above the Sembar Formation, was marine and reflects deposition at the western (passive)  
141 margin of the Indian plate.

142 The Sembar Formation is, therefore, overlain by the Lower Goru Member of the Goru  
143 Formation, i.e. the proven reservoir interval in the Sawan gas field (Fig. 2). The upper part of the  
144 Lower Goru Member is chiefly composed of shales, whereas its lower part comprises medium  
145 to coarse-grained sandstones with thin layers of shale and limestone. The lower portion of the  
146 reservoir interval can be subdivided into distinct sand intervals: A, B, C and D (Krois et al., 1998)  
147 (Figure 2). The deposition of these sand intervals took place in deltaic, shallow-marine  
148 environments during sea-level lowstands, when medium to coarse-grained sediment was  
149 deposited on top of the distal (shale and siltstone) strata of previous highstand systems tracts  
150 (HSTs) (Berger et al., 2009, Azeem et al., 2016).

151 Petrographically, intervals A and B can be classified as quartz-rich arenites (Berger et al.,  
152 2009). The C interval includes significant amounts of partially altered volcanic rock fragments  
153 and pore lining iron chlorite cement. Thus, the sands of interval C can be classified as sublithic  
154 to lithic arenites (McPhee and Enzendorfer, 2004; Berger et al., 2009; Azeem et al., 2016). Sands  
155 in the B and C intervals comprise the main gas reservoirs in the study area (Munir et al., 2011),  
156 showing high porosity (i.e. around 16 %) and permeability at depths between 3000–3500 m  
157 (Azeem et al., 2016). These two reservoir intervals of the Lower Goru Member are draped by  
158 transgressive shales and siltstones of the Upper Goru Member, which acts as a regional seal in  
159 the middle and lower Indus basins (Berger et al., 2009).

160

### 161 **3. Dataset and methods**

162

163 Data from three exploration wells (Sawan-01, Sawan-3B and Sawan-06) are used in this  
164 study to analyse the acoustic effects of the lithologic anisotropy created by interbedded shales in  
165 the C-sand reservoir. The rationale behind selecting the Sawan gas field as a case study results  
166 from the fact that it is located in the tectonically stable part of the Thar Platform, in the middle  
167 Indus basin. It also shows marked alternations of sands and shales, being a typical example of a  
168 VTI medium.

169 The workflow adopted in this work is shown in Figure 3. In a first instance, we analysed  
170 sand-shale distribution patterns in the main reservoir intervals using the methodology proposed  
171 by Thomas and Stieber (1975). In a second stage, rock physics modelling was undertaken using  
172 the Backus (1962) approach for dry composite porous media (sand-shale), used together with the  
173 relationships of Brown and Korringa (1975) and Wood (1955). These latter relationships allowed  
174 us to incorporate fluid effects on the mechanical properties of strata. The aim of the second stage  
175 of our analysis was to obtain (saturated) effective elastic properties for the Lower Goru reservoir

176 intervals (see also Jakobsen et al., 2003a, 2003b; Ali and Jakobsen, 2011a, 2011b; Ali et al.,  
177 2016).

178 In a third stage exact solutions of P-wave reflection coefficients, derived from Zoeppritz  
179 (1919) solutions for isotropic media and Daley and Horn's (1977) solutions for VTI media, were  
180 used to generate angle dependent reflection coefficients and seismic AVA data from the top of  
181 the reservoir, for both isotropic and anisotropic cases. In parallel, the Rüger's approximation  
182 (Rüger, 1998, 2002) was used for angle dependent reflection coefficients and seismic AVA data  
183 from the top of the reservoir, for both isotropic and anisotropic cases, over the Sawan reservoir  
184 intervals. Finally, a Bayesian inversion scheme was utilised to investigate the implications of  
185 isotropic and anisotropic AVA solutions on the estimation of porosity throughout the reservoir.

186

### 187 **3.1 Sand-Shale distribution analysis**

188

189 To understand shale distribution within reservoir sands is an integral part of forward  
190 modelling using rock physics templates (Ali et al., 2016). Prior to developing the appropriate  
191 rock physics model for AVA modelling, sand-shale distribution analyses are necessary to  
192 identify the type of shale(s) distributed within reservoir sands (Ali et al., 2016). This step  
193 improves confidence in the interpretation of sand-shale reservoirs because it helps interpreters to  
194 decide which geophysical approach is appropriate for a particular reservoir (Kurniawan, 2005).  
195 The distribution of shale within reservoir sands has a pronounced effect on reservoir production  
196 performance due to decreasing porosity values and variable saturations that derive from the  
197 presence of shales (Sames and Adrea, 2001; Ali et al., 2016). Hence, sand-shale distribution  
198 analyses require robust stratigraphic correlations based on gamma-ray log data (Figure 4).  
199 Gamma-ray curves are particularly helpful in the identification of shales within reservoir sand,  
200 and for detailed petrophysical analyses and correlations. The petrophysical interpretation of wells

201 (Sawan-01, Sawan-3B and Sawan-06) was carried out to determine key reservoir properties such  
202 as P-wave velocity ( $V_p$ ), S-wave velocity ( $V_s$ ), porosity ( $\phi$ ), density ( $\rho$ ), volume of shale ( $V_{sh}$ )  
203 and water saturation ( $S_w$ ) for the C-sand of the Lower Goru Member (Figures 5-7). The details  
204 of estimated reservoir parameters are given in Tables 1-3.

205 The parameters commonly required in sand-shale distribution analyses are volume of shale,  
206 porosity and water saturation, with the volume of shale being a critical parameter that controls  
207 the two latter (Saxena et al., 2006). Once these parameters are estimated, the Thomas-Stieber  
208 (1975) method in Figure 8 can be used to estimate shale distribution patterns (Saxena et al.,  
209 2006). The Thomas-Stieber (1975) method estimates shale distribution utilizing a cross-plot with  
210 volume of shale along the X-axis and total porosity along the Y-axis. The position of data points  
211 on the cross-plot allows the identification of the type(s) of shale distribution within sands.

212 Usually, shales are distributed through four different ways within sands: a) as laminae, b)  
213 through structures (faults, joints), c) dispersed in sands, and d) as any combinations of the three  
214 latter ways (Clavaud et al., 2005; Sams and Andrea, 2001). The results from sand-shale analyses  
215 undertaken for the three studied wells suggest that, in our study area, laminar and dispersed shales  
216 are distributed within reservoir sands (Figures 9-11).

217

### 218 **3.2. Forward Modelling**

219

220 The nonlinear forward problem is defined as:

221

$$222 \quad \mathbf{d} = G(\mathbf{m}). \quad (4)$$

223

224 In Equation (4),  $\mathbf{d}$  is a vector of observable quantities (angle-dependent reflection coefficients  
225 or seismic AVA data) and  $\mathbf{m}$  is a vector of model parameters required to be estimated over the

226 model space  $\mathbf{M}$  i.e.  $\mathbf{m} \in \mathbf{M}$ . The operator  $G$  is a forward modelling operator used for generating  
227 synthetic angle-dependent reflection coefficients, or seismic AVA data, via rock physics and  
228 seismic modelling. In the subsequent section we will discuss the rock physics modelling for a  
229 layered medium.

230

### 231 **3.2.1 Rock Physics modelling**

232

233 Rock physics models are important to correlate variations in reservoir properties (lithology,  
234 porosity, permeability, pore fluid, etc.) with changes in the velocities ( $V_p$ ,  $V_s$ ) and density ( $\rho$ )  
235 observed on well data (Uden et al., 2004). Rock physics models act as a bridge between  
236 geological properties (reservoir parameters) and geophysical data by upscaling the reservoir  
237 variables related to lithology, shale content and fluid parameters (Bachrach, 2006; Avseth et al.,  
238 2005). Rock physics also provide a realistic and systematic basis for seismic-attribute generation  
239 and interpretation (Avseth et al., 2005). In clastic reservoirs, shales are often found to behave  
240 elastically as transversely isotropic media with a vertical axis of symmetry (Jakobsen and  
241 Johansen, 1999, 2000). In forward models, rock physics models are used to calculate effective  
242 elastic properties from petrophysical properties estimated from wireline-log data.

243 Results of shale distribution analyses within the Sawan gas field reservoir sands show that  
244 laminar and dispersed shale types are distributed in the host medium. Such a medium can be  
245 modelled using anisotropic rock physics (Ali et al., 2016; Ali et al., 2015; Jakobsen et al., 2003;  
246 Sayers and Rickett 1997; Sayers, 1998; Backus, 1962). In this study, we follow the approach  
247 given by Backus (1962), which was typically designed for a layered medium (see Appendix-A).  
248 The fluid effects are incorporated via the Gassmann model for isotropic cases and via the Brown  
249 and Korringa (1975) model for anisotropic cases, in conjunction with the Wood (1955) model  
250 for homogenous saturations (Appendix-B).

251  
252  
253  
254  
255  
256  
257  
258  
259  
260  
261  
262  
263  
264  
265  
266  
267  
268  
269  
270  
271  
272  
273  
274  
275

### 3.2.2 Seismic amplitude variation with angle (AVA) modelling

Seismic AVA modelling is considered to be the most effective technique for reservoir characterisation. In practice, AVA studies are the method most widely used for gas detection, lithology identification and fluid parameter analyses (Feng and Bancroft, 2006). Seismic response of variations in effective elastic properties obtained through rock physics tools for sand-shale layers can be modelled using synthetic seismic AVA data. From the effective elastic properties as calculated above, angle-dependent reflection coefficients and seismic AVA data can be generated using the exact Zoeppritz (1919) formulation for isotropic media, and the Daley and Horn's (1977) exact methods for anisotropic (VTI) media. We also tested the Rüger (2002) approximation for the generation of reflection coefficients for both isotropic and VTI media. The rationale behind only selecting Rüger's approximation for isotropic and VTI media is that the Rüger's technique is only linearised in terms of small contrasts in medium parameters, without having any additional assumption on Poisson's or  $V_p/V_s$  ratios (Rüger, 2002).

#### 3.2.2.1 P-wave reflection coefficient for isotropic media

The exact Zoeppritz (1919) empirical relation (see Equation 5) allows us to calculate the PP-wave reflection coefficients ( $R_{PP}$ ) of a rock as a function of the incidence angle from the top of an isotropic medium, which can be represented as a system of linear equations given as (Pujol, 2003):

$$AX = B, \tag{5}$$

Where:

$$276 \quad A = \begin{bmatrix} -\text{Sine} & \text{Cos}f & \text{Sine}' & \text{Cos}f' \\ \text{Cose} & \sin f & \cos e' & -\text{Sin}f' \\ \text{Sin } 2e & -\frac{\alpha}{\beta} \text{Cos } 2f & \frac{\rho'\alpha}{\rho\alpha} \left(\frac{\beta'}{\beta}\right)^2 \text{Sin } 2e' & \frac{\rho'\alpha}{\rho\beta'} \left(\frac{\beta'}{\beta}\right)^2 \text{Cos } 2f' \\ -\text{Cos } 2f & -\frac{\beta}{\alpha} \text{Sin } 2f & \frac{\rho'\alpha}{\rho\alpha} \text{Cos } 2f' & -\frac{\rho'\beta'}{\rho\alpha} \text{Sin } 2f' \end{bmatrix}, \quad (6)$$

$$277 \quad X = \begin{bmatrix} R_{PP} \\ T_{PP} \\ R_{PS} \\ T_{PS} \end{bmatrix}, \quad (7)$$

$$278 \quad \text{and } B = \begin{bmatrix} \text{Sine} \\ \text{Cose} \\ \text{Sin } 2e \\ \text{Cos } 2f \end{bmatrix}. \quad (8)$$

279

280 The unknown vector  $X$  can be obtained by:

281

$$282 \quad X = A^{-1}B. \quad (9)$$

283

284 In these equations,  $\alpha$ ,  $\beta$ ,  $\rho$ ,  $e$  and  $f$  are the P-wave velocity, S-wave velocity, density, P-wave  
 285 transmission angle, and SV-wave transmission angle of the upper half space. Conversely,  $\alpha'$ ,  $\beta'$ ,  
 286  $\rho'$ ,  $e'$  and  $f'$  are the P-wave velocity, S-wave velocity, density and P-wave reflection angle, and  
 287 SV-wave reflection angle of the lower half space.

288

### 289 3.2.2.2 Formulation of PP-wave reflection coefficients for VTI media

290

291 The exact algebraic solution for reflection/transmission coefficients ( $R, T$ ) of plane incident  
 292 P-waves in a VTI medium, developed by Daley and Horn (1977), is used in this work. The  
 293 concise form of the exact solution of P-wave reflection coefficients for a VTI medium ( $R_{PP}^{VTI}$ ),  
 294 in matrix form, is given below (Graebner, 1992; Rüger, 2002):

$$295 \quad MR = b, \quad (10)$$

296 where  $\mathbf{b} = [-m_{11}, -m_{21}, m_{31}, m_{41}]^T$ , (11)

297 and  $\mathbf{R} = \begin{bmatrix} R_{PP}^{VTI} \\ R_{PS}^{VTI} \\ T_{PP}^{VTI} \\ T_{PS}^{VTI} \end{bmatrix}$ . (12)

298 By using Cramer's rule, the solution for unknown vector  $\mathbf{R}$  can be expressed in its analytic form  
 299 as:

300  $\mathbf{R} = \frac{1}{\det \mathbf{M}} \begin{bmatrix} M_{11} & M_{12} & M_{13} & M_{14} \\ M_{21} & M_{22} & M_{23} & M_{24} \\ M_{31} & M_{32} & M_{33} & M_{34} \\ M_{41} & M_{42} & M_{43} & M_{44} \end{bmatrix}^T \mathbf{b}$ . (13)

301 The values of matrices  $\mathbf{M}$  and  $\mathbf{b}$  are given by Rüger (2002), Graebner (1992) and Daley and Horn  
 302 (1977).

303

### 304 3.2.2.3 Approximations for P-wave reflection coefficients

305

306 We also investigate the accuracy of Rüger's (2002) approximation for both isotropic and VTI  
 307 media with the exact solutions given by Zeppritz's (1919) and Daley and Horn's (1977).  
 308 Rüger's approximation for isotropic media is given below (Rüger, 2002):

309

310  $R_{PP}^{iso}(i) = \frac{1}{2} \frac{\Delta Z}{Z} + \frac{1}{2} \left\{ \frac{\Delta V_{P0}}{\bar{V}_{P0}} - \left( \frac{2\bar{V}_{S0}}{\bar{V}_{P0}} \right)^2 \frac{\Delta G}{G} \right\} \sin^2 i + \frac{1}{2} \left\{ \frac{\Delta V_{P0}}{\bar{V}_{P0}} \right\} \sin^2 i \tan^2 i$ . (14)

311

312 Where  $Z$  is the P-wave impedance,  $G$  is the shear wave modulus,  $V_{P0}$  is the vertical P-wave  
 313 velocity, and  $V_{S0}$  is the vertical shear-wave velocity. The character delta ( $\Delta$ ) stands for contrasts  
 314 across an interface ( $\Delta Z = Z_2 - Z_1$ ), and the bar over a symbol represents its average ( $\bar{Z} = \frac{Z_1+Z_2}{2}$ ).  
 315 Subscript 1 corresponds to the upper layer and subscript 2 denotes the lower layer. Rüger's  
 316 approximation for the generation of reflection coefficients as a function of incidence angle ( $i$ ),  
 317 in the case of VTI media (Rüger, 2002), is written as:

318

$$319 \quad R_{PP}^{VTI}(i) = \frac{1}{2} \frac{\Delta Z}{\bar{Z}} + \frac{1}{2} \left\{ \frac{\Delta V_{P0}}{\bar{V}_{P0}} - \left( \frac{2\bar{V}_{S0}}{\bar{V}_{P0}} \right)^2 \frac{\Delta G}{G} + \Delta\delta \right\} \sin^2 i + \frac{1}{2} \left\{ \frac{\Delta V_{P0}}{\bar{V}_{P0}} + \Delta\varepsilon \right\} \sin^2 i \tan^2 i. \quad (15)$$

320

321 The additional terms  $\varepsilon$  and  $\delta$  are Thomsen's (1985, 1996) anisotropy parameters for VTI  
 322 media.

323

### 324 **3.3 Inverse modelling**

325

326 In Bayesian settings, the solution of the inverse problem is given by the posterior probability  
 327 distribution  $q(\mathbf{m} | \mathbf{d})$  applied over the model space  $M$ . In essence,  $q(\mathbf{m} | \mathbf{d})$  carries all the  
 328 information about the model originating from the likelihood  $L(\mathbf{m})$  and *a priori* probability  
 329 density function  $p(\mathbf{m})$ . Bayes' theorem allows to relate  $q(\mathbf{m} | \mathbf{d})$  with  $L(\mathbf{m})$  and  $p(\mathbf{m})$  given  
 330 as (Aster et al., 2005):

331

$$332 \quad q(\mathbf{m} | \mathbf{d}) \propto L(\mathbf{m})p(\mathbf{m}). \quad (16)$$

333

334 Here  $\propto$  is the sign of proportionality. The solution of the posterior distribution can be written  
 335 in a compact form as (Aster et al., 2005; Tarantola, 2005):

336

337 
$$q(\mathbf{m} | \mathbf{d}) = N. e^{-J(\mathbf{m})}, \quad (17)$$

338

339 where  $N$  is the normalization constant. The functional form of the objective function  $J(\mathbf{m})$ ,  
340 required to be minimised in the case of Gaussian statistics, and an uninformative prior  
341 distribution, is given by Aster et al., (2005) as:

342

343 
$$J(\mathbf{m}) = \min \sum_{i=1}^n \frac{((G(\mathbf{m}))_i - d_i)^2}{2\sigma^2}. \quad (18)$$

344

345 Here,  $\sigma$  is the standard deviation of the measured seismic data. The rationale behind assuming  
346 an uninformative prior distribution is that we do not intend to constrain our inversion scheme by  
347 incorporating *a priori* information (obtained mostly from log/core/laboratory data) about the  
348 model parameters. There are different methods available for the evaluation of  $q(\mathbf{m} | \mathbf{d})$ , most of  
349 which are described in Ali et al. (2011a; 2011b and 2015).

350

#### 351 **4. Numerical results and discussion**

352

353 In this work, we analyse the effects created by sand-shale anisotropy on AVA response with  
354 the help of rock physics modelling. In parallel, we present a comparison of exact and approximate  
355 AVA solutions for isotropic and anisotropic scenarios. Before applying rock physics modelling  
356 to layered media, it is very important to identify the type of shale distribution within reservoir  
357 sands, e.g. laminar, structural, dispersed, and so on. For this same purpose, we followed the  
358 approach presented in Section 3.1 for the C-sand reservoir unit (Lower Goru Member) drilled by

359 wells Sawan-01, Sawan-3B and Sawan-06. Reservoir properties are estimated through  
360 petrophysical analyses of well log data acquired in the Sawan field and results are presented in  
361 Figures 5-7 and in Tables 1-2.

362 The analysis of shale distribution suggests that the C-sand comprises laminated and dispersed  
363 shale types (Figures 8-11). Thus, the Lower Goru C-sand may be a potential candidate to be  
364 characterised as a VTI medium, rather than isotropic. Laminar shales in the C-sand reservoir  
365 comprise thin layers of allogenic clays and do not control effective porosity, water saturation, or  
366 the horizontal permeability of rock. However, they significantly change vertical permeability  
367 (Kurniawan, 2005). Each lamina differs in thickness, in a way that the amounts of sand, silt and  
368 clay in the layer are repeated as depositional sequences (or cycles) under dual flow regimes that  
369 denote contrasts in energy level.

370 The saturated effective elastic properties for isotropic and VTI media are obtained using the  
371 methodology discussed in section 3.2. The input to our rock physics modelling, in the form of  
372 elastic and reservoir properties of the Lower Goru C-sand, intra-reservoir shale layers and  
373 overburden strata, is extracted from the petrophysical analyses summarised in Table 3. The  
374 elastic properties of solid mineral (quartz) and fluid (water and gas), required to generate AVA  
375 data, are given in Table 4.

376 For the generation of isotropic angle-dependent reflection coefficient curves are used the exact  
377 solution of Zeoppritz (1919) for isotropic media, and Daley and Horn's (1977) solution for VTI  
378 media. Rüger's (2002) approximation is also used for both isotropic and VTI media to investigate  
379 the accuracy of exact and approximate solution of P-wave reflection coefficients as a function of  
380 incidence angle.

381 The angle dependent reflection coefficient (RC) curves are key to explain the main results in  
382 this work. We demonstrate in Figs. 12-14 that the intercept (normal incidence i.e. zero offset, P-  
383 wave reflectivity) and slope of the curve (gradient) indicate how the amplitude of RC changes  
384 with angle/offset. The gradient of each RC curve is almost the same, but there are small

385 differences in the magnitude of angle-dependent PP-reflection coefficients when comparing the  
386 isotropic and anisotropic cases (Figures 12-14). If we examine variations in RC based upon  
387 isotropy and anisotropy it is obvious that, in the Sawan-01 well, only small differences can be  
388 observed between isotropic and anisotropic RC curves (Figure 12). This clearly demonstrates  
389 that strata drilled in Sawan-01 have a weak anisotropy ( $\epsilon = 0.0214$ ,  $\delta = 0.0306$ ,  $\gamma = 0.0186$ ). In  
390 Sawan-3B, there are insignificant variations between isotropic and anisotropic RC curves (Figure  
391 13). Finally, for Sawan-06 there is a significant variation in RC curves when comparing the  
392 isotropic and anisotropic cases (Figure 14). More importantly, if we relate these variations in RC  
393 curves with varying shale content, we can conclude that the wells with comparatively thick shale  
394 layers show substantial variations between their isotropic and anisotropic RC curves. The best  
395 example is, naturally, the RC response documented in well Sawan-06 (Figure 14; see also thick  
396 shale content marked in yellow in Figure 4).

397 We observe that AVA data is moderately sensitive to the anisotropy of the medium. In  
398 essence, our results confirm that little or no effects created by anisotropy upon reflection curves  
399 are diagnostic of very weakly anisotropic media. Significantly, as shales are strongly anisotropic  
400 and heterogeneous (Kumar et al., 2012), exploration well(s) that encountered thick shale layers  
401 in the study area show clear variations between the behaviour of isotropic and anisotropic angle  
402 dependent PP-reflection coefficients (Figure 14). Based on data from the three interpreted wells  
403 (Sawan-01, Sawan-3B and Sawan-06), shale anisotropy increases proportionally to shale content,  
404 and the effect of this same shale anisotropy upon reflection curves becomes more pronounced.  
405 As such, it is advisable to predict anisotropy in a medium during AVA studies, especially when  
406 thick allogenic shale layers are present in reservoir successions.

407 The investigation of Ruger (2002) approximation's accuracy for both isotropic and VTI media  
408 reveal that the predicted magnitude of reflection coefficients is significantly different in all the  
409 three studied wells, at large offsets. Also, the gradient predicted by the Ruger (2002)  
410 approximation is high when compared to the exact solutions.

411 For seismic AVA response in isotropic and VTI media, angle-dependent reflection  
412 coefficients are convolved with the source (Ricker) wavelet (Figures 15-17). It can be observed  
413 from our approach that the amplitude of synthetic AVA gathers show a decreasing trend with  
414 increasing angle of incidence. The difference between exact and approximate solutions is more  
415 pronounced in the magnitude of predicted seismic AVA amplitude values (Figures 15-17).

416 The AVA response of VTI media is sensitive to contrasts in Thomsen's anisotropic  
417 parameters,  $\epsilon$  and  $\delta$ , across the interface (Blangy 1994; Margesson and Sondergeld, 1999). As  
418 also identified by Daley and Horn (1977), generally P-P reflections indicate that the smaller the  
419 contrast in isotropic properties ( $V_P$ ,  $V_s$ ,  $\rho$ ), and the larger the contrast in  $\delta$  (variation in P-wave  
420 velocity with phase angle for near vertical propagation) across a reflection interface, the greater  
421 are the effects of anisotropy on AVA signatures. Contrasts in  $\delta$  are most important under small-  
422 to-medium angles of incidence, as previously reported in Banik (1987), whereas contrasts in  $\epsilon$   
423 (fractional difference between the horizontal and vertical P-wave velocities) can have a strong  
424 influence on amplitudes for the larger angles of incidence ( $21^\circ$ ) commonly used in exploration  
425 seismic data. The increasing trend in gradients is more pronounced at far offsets ( $21^\circ$  to  $40^\circ$ ),  
426 revealing an increasing sensitivity in terms of anisotropy and isotropy with increasing offset  
427 angles.

428 The AVA modelling also proves a strong relationship between porosity and reflection  
429 coefficient for all offset ranges. Therefore, in order to check the accuracy of exact and  
430 approximate solutions for P-wave reflection coefficients in AVA inversion, we tried to recover  
431 true reservoir porosity distribution (with 20% uncertainty) under the Bayesian settings discussed  
432 in Section 6. For this purpose, a correlated Gaussian field was generated representing the true  
433 porosity (Buland and Omre, 2003) distribution throughout the reservoir within  $100 \times 100$  grid  
434 blocks (Figure 18). Later, a AVA modelling approach (exact/approximate VTI or  
435 exact/approximate isotropic) was performed using a maximum-a-posteriori (MAP) solution. The

436 results suggest that the exact VTI solution recovers the porosity trends with much more accuracy  
437 when compared to all other solutions, under significant noise conditions (Figure 18).

438

## 439 **5. Conclusions**

440 In industry, seismic AVA/AVO techniques are being increasingly used for amplitude-based  
441 reservoir characterisation, but frequently assume that subsurface media are isotropic. Seismic  
442 anisotropy is known to have a first order effect on AVA modelling but this effect is often ignored  
443 during AVA studies, providing significant errors when describing reservoir intervals. In this  
444 work we analyse the effects of anisotropy on AVA modelling and inversion for a sand-shale  
445 reservoir in the Sawan gas field, Pakistan. The main conclusions of this work are as follows:

446

447 a) AVA modelling shows that anisotropy effects are more pronounced in stratigraphic  
448 intervals where interbedded shales are relatively thick within reservoir sand (Sawan-06 well).  
449 The exact/approximate isotropic or VTI solutions show smaller variations in the presence of thin  
450 interbedded shale layers within reservoir sands.

451 b) The exact solution for VTI media provided by Daley and Horn's (1977) is one with the  
452 highest potential for performing AVA inversion in sand-shale media with weak to strong  
453 anisotropy. We have demonstrated this fact by completing a numerical synthetic experiment for  
454 recovering porosity distributions through the Lower Goru reservoir.

455 c) The choice of approximate solution(s) for AVA modelling is crucial in any workflow since,  
456 in most cases, there is a significant difference in the predictions of magnitude of reflection  
457 coefficients, and gradient of the reflection curves, resulting from distinct approximate solutions.  
458 As suggested by our own AVA modelling results, the Rüger's approximation is significantly  
459 different to other techniques when considering the magnitude and gradient of reflection curves.  
460 This fact can create additional uncertainty to the use of AVA inversion techniques in the  
461 characterisation of shale-sand reservoirs.

462

463 **Acknowledgments**

464 Dr. Aamir Ali (Advisor) and Hafiz Mubasher Anwer (PhD Scholar) would like to thank the  
465 Higher Education Commission (HEC) of Pakistan for providing the necessary funding needed to  
466 complete this research work. The authors are also pleased to the Director General Petroleum  
467 Concessions (DGPC), Ministry of Petroleum and Natural Resources, Government of Pakistan  
468 and joint venture partners of Sawan gas field for providing data and other required material to  
469 complete this work. TA thanks Cardiff University for their support to a visiting staff scheme set  
470 with HMA. Reviewers and Editor M. Faure are acknowledged for their constructive feedback.

471

472 **References**

473 Afzal, J., Kuffner, T., Rahman, A., Ibrahim, M., 2009. Seismic and well-log based sequence  
474 stratigraphy of the early Cretaceous, Lower Goru "C" sand of the Sawan gas field, middle Indus  
475 Platform, Pakistan. Annual Technical Conference, Islamabad.

476 Ahmad, N., Fink, P., Sturrock, S., Mahmood, T., Ibrahim, M., 2004. Sequence stratigraphy as  
477 predictive tool in Lower Goru fairway, Lower Middle Indus Platform, Pakistan. PAPG-SPE  
478 ATC, 85-105.

479 Alam, I., Azhar, A.M., Khan, M.W., 2014. Frontal structural style of the Khisor Range, northwest  
480 of Bilot: Implications for hydrocarbon potential of the north-western Punjab foredeep, Pakistan.  
481 Journal of Himalayan Earth Sciences, Volume 47, Issue No. 1, 87-98.

482 Ali, A., Anwer, H.M., Hussain, M., 2015. A comparisonal study in the context of seismic fracture  
483 characterization based on effective stiffness and compliance methods, Arab. J. of Geosci., DOI  
484 :10.1007/s12517-014-1478-8

485 Ali, A., Jakobsen, M., 2011a. On the accuracy of Rüger's approximation for reflection  
486 coefficients in HTI media: implications for the determination of fracture density and orientation  
487 from seismic AVAZ data. *Journal of Geophysics and Engineering*, issue No. 8, 372-393.

488 Ali, A., Jakobsen, M., 2011b. Seismic characterization of reservoirs with multiple fractures sets  
489 using velocity and attenuation anisotropy data, *Journal of Applied Geophysics*, Issue No.75, 590-  
490 602.

491 Ali, A., Shahraini, A., Jakobsen, M., 2011. Improved characterization of fault zones by  
492 quantitative integration of seismic and production data, *Journal of Geophysics& Eng.* Issue 8,  
493 259–274.

494 Ali, A., Zubair, Hussain, M., Rehman, K., Toqeer, M., 2016. Effect of Shale Distribution on  
495 Hydrocarbon Sands Integrated with Anisotropic Rock Physics for AVA Modelling: A Case  
496 Study, *Acta Geophysica*, vol. 64, issue No. 4, 1139-1163.

497 Almutlaq, M.H., Margrave, G.F., 2010. Tutorial: AVO inversion, *CREWES Research Report*,  
498 Vol. 22, 1-23.

499 Asim, S., Zhu, P., Qureshi S.N., Naseer, M.T., 2015. A case study of Precambrian to Eocene  
500 sediments' hydrocarbon potential assessment in Central Indus Basin of Pakistan, *Arabian Journal*  
501 *of Geosciences*, ISSN 1866-7511, DOI 10.1007/s12517-015-1988-z.

502 Aster, R.C., Borchers, B., Thurber, C.H., 2005. *Parameter Estimation and Inverse Problems*.  
503 ISBN: 0-12-065604-3, Elsevier Academic Press, Amsterdam.

504 Avseth, P., Mukerji, T., Mavko, G., 2005. *Quantitative seismic interpretation: Applying rock*  
505 *physics tools to reduce interpretation risk*. ISBN: 0-13-978-0-521-81601-7, Cambridge  
506 University Press, UK.

507 Azeem, T., Yanchun, W., Khalid, P., Xueqing, L., Yuan, F., Lifang, C., 2016. An application of  
508 seismic attributes analysis for mapping of gas bearing sand zones in the Sawan gas field Pakistan.  
509 *Acta Geod. Geophys*, DOI 10.1007/s40328-015-0155-z.

510 Bachrach, R., 2006. Joint estimation of porosity and saturation using stochastic rock-physics  
511 modelling. *Geophysics*, 71(5), 53–63.

512 Backus, G.E.,1962. Long-wave elastic anisotropy produced by horizontal layering. *J.*  
513 *Geophysics, Res.*, issue No.67, 4427-4440.

514 Ball, G., 1995. Estimation of anisotropy and anisotropic 3-D Prestack depth migration, offshore  
515 Zaire. *Geophysics*, issue No. 60, 1495-1513.

516 Banik, N. C., 1987. An effective anisotropy parameter in transversely isotropic media.  
517 *Geophysics*, 52(12), 1654-1664.

518 Berger, A., Gier, S., Krois, P., 2009. Porosity-preserving chlorite cements in shallow-marine  
519 volcanoclastic sandstones: evidence of the Sawan gas field Pakistan. *AAPG Bull* 93(5), 595-615.

520 Besheli, S. A., Urosevic, M., Li, R., 2005. The effect of seismic anisotropy on reservoir  
521 characterization. *SEG Annual Meeting Houston, USA*.

522 Blangy, J.P.,1992. Anisotropy and AVO in TI media, an overview: Joint SEG. In EAEG summer  
523 research workshop, *Expanded Abstracts*, Vol. 60, 1-605.

524 Blangy, J.P.,1994. AVO in transversely isotropic media-An overview, *Geophysics*, Vol 59, No.5,  
525 775-781.

526 Brajanovski, M., Nadri, D., Gurevich, B. Bona, A., 2009. Stress induced anisotropy in sandstone  
527 reservoir and shale overburden - AVO modeling. *International Geophysical Conference and*

528 Exposition, Beijing, China, 24–27 April, 194-194. ISBN: 978-1-56080-284-6 doi:  
529 10.1190/1.3603719.

530 Brown, R.J.S., Korringa, J., 1975. On the dependence of elastic properties of a porous rock on  
531 the compressibility of the pore fluid. *Geophysics* 40, 608–616.

532 Buland, A., Omre, H., 2003. Joint AVO inversion-wavelet estimation and noise level estimation  
533 using a spatially coupled and hierarchical Bayesian Model, *Geophysical Prospecting*, 51, 531-  
534 550.

535 Chao G., Cadore, T., Deplante, C., Gratzer, O., 2012. Detailed AVA analysis of a class IIp  
536 reservoir in presence of VTI shale anisotropy. A case study from offshore West Africa. SEG  
537 Annual Meeting, Las Vegas, DOI:10.1190/segam2012-1280.1.

538 Chengzao, J., Min, Z., Yongfeng, Z., 2012. Unconventional Hydrocarbon Resources in China  
539 and the Prospect of Exploration and Development. *Petroleum Exploration and Development*, v.  
540 39/2, 129-136.

541 Clavaud, J.B., Nelson, R., Guru, U.K., Wang, H., 2005. Field example of enhanced hydrocarbon  
542 estimation in thinly laminated formation with a triaxial array induction tool: A laminated sand-  
543 shale analysis with anisotropic shale. SPWLA 46th Annual Logging Symposium, 26-29 June,  
544 New Orleans, USA.

545 Crampin, S., Chesnokov, E.M., Hipkin, R.G., 1984. Seismic Anisotropy- the state of the art: II.  
546 *Geophysics. J. Int. issue* 76(1), 1-16.

547 Da Silva, N.V., Ratcliffe, A., Vinje, V., Conroy, G., 2016. A new parameter set for anisotropic  
548 multiparameter full-waveform inversion and application to a North Sea dataset. *Geophysics*, Vol.  
549 81, issue No. 4, U25–U38.

550 Daley, P.F., Horn, F., 1977. Reflection and transmission coefficients for transversely isotropic  
551 media. Bull. Seis. Soc. Am., issue No. 67, 661-675.

552 Das, I., Zoback, M.D., 2013. Long-period, long-duration seismic events during hydraulic  
553 stimulation of shale and tight-gas reservoirs Part 1: Waveform characteristics. Geophysics, Vol.  
554 78, No. 6, KS97-KS108.

555 English, J.M., Lunn, G.A., Ferreira, L., Yacu, G., 2015. Geologic evolution of the Iraqi Zagros  
556 and its influence on the distribution of hydrocarbons in the Kurdistan region. AAPG Bulletin,  
557 V.99, No.2, 231-272, DOI: 10.1306/06271413205.

558 Feng, H., Bancroft, J.C., 2006. AVO principles, processing and inversion. CREWES Research  
559 Report, Vol. 18, 1-19.

560 Fink, P., Schuh, M., Ahmad, N., Koehazy, R., 2004. Can the American Securities and Exchange  
561 Commission and the central limit theorem ever become friends? A practical proposal for  
562 reconciliation from OMV's Sawan Reserves Estimation exercise. PAPG/SPE Annual Technical  
563 Conference, 8-9 October, Islamabad, Pakistan.

564 Floridaia, C., Teles, N.T., 1998. Effects of anisotropy in the AVO analysis. SEG Technical  
565 Program, Expanded Abstracts, 212-215. doi:10.1190/1.1820378.

566 Gassmann, F., 1951. Über die Elastizität poröser Medien. Viertel.Naturforsch.Ges. Zürich, 96, 1-  
567 23.

568 Goodway, B., Perez, M., Varsek, J., Abaco, C., 2010. Seismic petrophysics and isotropic-  
569 anisotropic AVO methods for unconventional gas exploration. The Leading Edge, 29(12), 1500-  
570 1508. Doi: 10.1190/1.3525367.

571 Graebner, M., 1992. Plane-wave reflection and transmission coefficients for a transversely  
572 isotropic solid. *Geophysics*, 57(11), 1512-1519, doi:10.1190/1.1443219.

573 Grechka, V., 1998. AVO analysis in finely layered azimuthally anisotropic media. SEG Technical  
574 Program, Expanded Abstracts. 1649-1652. doi: 10.1190/1.1820238.

575 Iqbal, M.W.A., Shah, S.M.I., 1980. A guide to the stratigraphy of Pakistan, Geological Survey  
576 of Pakistan, Records. Geol. Surv. Pak. Quetta, 53-34.

577 Jakobsen, M., Johansen, T.A., 1999. A test of ANNIE based on ultrasonic measurements on a  
578 shale. *J. Seis. Explor.* issue No. 8, 77-89.

579 Jakobsen, M., Hudson, J.A., Johansen, T.A., 2003a. T-matrix approach to shale acoustics.  
580 *Geophysical Journal International*, Issue No.154, 533-558.

581 Jakobsen, M., Johansen, T.A., 2000. Anisotropic approximations for mud rocks: A seismic  
582 laboratory study. *Geophys.* **65**, 1711-1725.

583 Jakobsen, M., Johansen, T.A., McCann, C., 2003b. The acoustic signature of fluid flow in  
584 complex porous media. *Journal of Applied Geophysics*, 54, 219-246.

585 Jinhu, D., He, L., Desheng, M., Jinhua, F., Yuhua, W., Zhou, T., 2014. Discussion on effective  
586 development techniques for continental tight oil in China. *Petroleum Exploration and*  
587 *Development*, Volume 41, Issue 2, 217-224.

588 Kadri, I.B., 1995. *Petroleum geology of Pakistan: Pakistan Petroleum Limited. Graphic*  
589 *Publishers Karachi.*

590 Katz, B., Lin, F., 2014. Lacustrine Basin unconventional Resource Plays: Key differences.  
591 *Marine and Petroleum Geology*, Volume 56, 255-265.

592 Kim, K.Y., Wroldstad, K.H., Aminzadeh, F., 1993. Effects of Transverse Isotropy on P-wave  
593 AVO for gas sands. *Geophysics*, 58, 883-888.

594 Krois P, Mahmood T, Milan, G., 1998. Miano field, Pakistan a case history of model driven  
595 exploration. Proceedings of the Pakistan Petroleum Convention, Pakistan Association of  
596 Petroleum Geologists Islamabad, 111-131.

597 Kumar, D., Hoversten, G.M., 2012. Geophysical model response in a shale gas. 9th Biennial  
598 international conference & Exposition on Petroleum Geophysics, Hyderabad, India.

599 Kurniawan, F., 2005. Shaly Sand Interpretation Using CEC-Dependent Petrophysical  
600 Parameters, MS Dissertation, Louisiana State University and Agricultural and Mechanical  
601 College.

602 Leaney, W.S., 1993. AVO and anisotropy from logs and walkaways. *Exploration Geophysics*,  
603 24, 623-630.

604 Li, V., Tsvankin, I., Alkhalifah, T., 2016. Analysis of RTM extended images for VTI media  
605 *Geophysics*, Vol. 81, NO.3, S139–S150, DOI: 10.1190/GEO2015-0384.1.

606 Luo, X., Lin, Y., Wu, L., Yao, F., 2005. Estimation of anisotropy parameters in VTI Media from  
607 surface P-wave seismic data and VSP in Tarim Basin, China. SEG Annual Meeting, Houston.  
608 178-181.

609 Margesson, R.W., Sondergeld, C.H., 1999. Anisotropy and amplitude versus offset: a case  
610 history from the West of Shetlands. Proceedings of the 5<sup>th</sup> Conference, 635-643. Petroleum  
611 Geology '86 Ltd. Published by the Geological Society, London.

612 Mavko, G., Mukerji, T., Dvorkin, J. 2009. *The Rock Physics Handbook: Tools for Seismic*  
613 *Analysis in Porous Media*. Cambridge University Press, UK.

614 McGlade, C., Speirs, J., Sorrell, S., 2012. A review of regional and global estimates of  
615 unconventional gas resources. A report to the Energy Security Unit of the Joint Research Centre  
616 of the European Commission.

617 McPhee, C.A., Enzendorfer, C.K., 2004. Sand management solutions for high-rate gas wells,  
618 Sawan field. SPE, Sindh.

619 Munir, K., Iqbal, M.A., Farid, A., Shabih, S.M. 2011. Mapping the productive sands of Lower  
620 Goru Formation by using seismic stratigraphy and rock physical studies in Sawan area, southern  
621 Pakistan: a case study. *Journal of Petroleum Exploration & Production Technology*, issue No.1,  
622 33-42, doi:10.1007/s13202-011-0003-9.

623 Nourollah, H., Urosevic M., Keetley, J., 2015. Seal potential of shale sequences through seismic  
624 anisotropy: Case study from Exmouth Sub-basin, Australia. *Society of Exploration  
625 Geophysicists Vol. 3, Issue No. 4, T257-T267.*

626 Pujol, J., 2003. *Elastic Wave Propagation and Generation in Seismology*. ISBN 0-521-52046-0,  
627 Cambridge University Press, UK, 160-161.

628 Quadri, V.N., Shuaib, M.,1986. Hydrocarbon prospects of Southern Indus Basin, AAPG  
629 Bulletin, v. 70, pp.730–747.

630 Rodriguez, K., Hodgson, N., Hewitt, A., 2016. The future of oil exploration. *First Break*, Vol 34,  
631 issue No 2, 95-101.

632 Rüger, A., 2002. *Reflection Coefficients and Azimuthal AVO Analysis in Anisotropic Media:*  
633 *Geophysical Monograph Series, No. 10, Society of Exploration Geophysics.*

634 Rüger, A.,1998. Variation of P-wave reflectivity with offset and azimuth in anisotropic media.  
635 *Geophysics*, issue Nno.63, 935-947.

636 Sams, M.S., Andrea, M., 2001. The effect of clay distribution on the elastic properties of  
637 sandstones. *Geophysical Prospecting*, 49,128-150.

638 Saxena, K., Tyagi, A., Klimentos, T., Morriss, C., Mathew, A. 2006. Evaluating Deepwater Thin-  
639 Bedded Reservoirs with the RT Scanner. Petromin, Kaula Lumpur.

640 Sayers, C.M. 2013. Rock Physics for Reservoir Exploration, Characterisation and Monitoring.  
641 *Geophysical Prospecting*, 61, 251–253. doi: 10.1111/1365-2478.12034.

642 Sayers, C.M., 1998. Long-wave seismic anisotropy of heterogeneous reservoirs, *Geophysical J.*  
643 *Int.* 132, 667-673.

644 Sayers, C.M., Rickett, J.E., 1997. Azimuthal variation in AVO response for fractured gas sands,  
645 *Geophysical Prospecting*, 45, 165-182.

646 Shahraini, A., Ali, A., Jakobsen, M. 2011. Seismic history matching in fractured reservoirs using  
647 a consistent stiffness-permeability model: Focus on the effects of fracture aperture, *Geophysical*  
648 *Prospecting*, 59, 492-505.

649 Sone, H., Zoback, M.D., 2013. Mechanical properties of shale-gas reservoir rocks Part 2: Ductile  
650 creep, brittle strength, and their relation to the elastic modulus. *Geophysics* , Vol. 78, No. 5,  
651 D393-D402.

652 Tarantola, A., 2005. *Inverse Problem Theory and Methods for Model Parameter Estimation.*  
653 Society for Industrial and Applied Mathematics, USA.

654 Thomas, E.C., Stieber S.J., 1975. The distribution of shale in sandstones and its effect on  
655 porosity. SPWLA 16th Annual Logging Symp., 4-7 June 1975.

656 Thomsen, L., 1995. Elasticity anisotropy due to aligned cracks in porous rock, *Geophysical*  
657 *Prospecting*, 43, 805-829.

658 Thomsen, L., 1986. Weak elastic anisotropy. *Geophysics*, 51(10), 1954-1966.

659 Tsvankin, I., 1997a. Anisotropic parameters and P-wave velocity for orthorhombic media  
660 *Geophysics*, 62, 1292–1309.

661 Tsvankin, I., 1997b. Reflection move out and parameter estimation for horizontal transverse  
662 isotropy. *Geophysics*, issue No.62, 614-629.

663 Tyagi, A.K., Guha, R., Voleti, D., Saxena, K., 2009. Challenges in The Reservoir  
664 Characterization of a Laminated Sand Shale Sequence. 2nd SPWLA-India Symposium,  
665 November 19-20.

666 Uden, R., Dvorkin, J., Walls, J., Carr, M., 2004. Lithology substitution in a sand/shale sequence.  
667 ASEG 17<sup>th</sup> Geophysical Conference and Exhibition, Sydney.

668 Wandrey, C.J., Law, B.E., Shah, H.A., 2004. Sembar Goru/Ghazij composite total petroleum  
669 system Indus and Sulaiman-Kirthar geologic Provinces Pakistan and India. US Geological  
670 Survey, USA; Geological Survey Bulletin.

671 Wang, L., Dai, H., Li, X.Y., 2006. Estimating anisotropic parameters from PS converted-wave  
672 data: a case study. British Geological Survey, Xianyi Sun, Petro China, Daqing Oil Field.

673 Wang, Y., 2011. Seismic anisotropy estimated from P-wave arrival times in cross hole  
674 measurements. *Geophysical Journal International*, 184, 1311-1316.

675 Wood, A.W., 1955. *A Textbook of Sounds*, New York, McMillan Co. USA.

676 Wright, J., 1987. The effects of transverse isotropy on reflection amplitude versus offset.  
677 Geophysics, 52, 564-567.

678 Xu, S., Wu, X., Huang, X., Yin, H., 2005. Evaluation of Anisotropic Rock Properties in  
679 Sedimentary Rocks from well log. Offshore Technology Conference Houston, TX, USA.

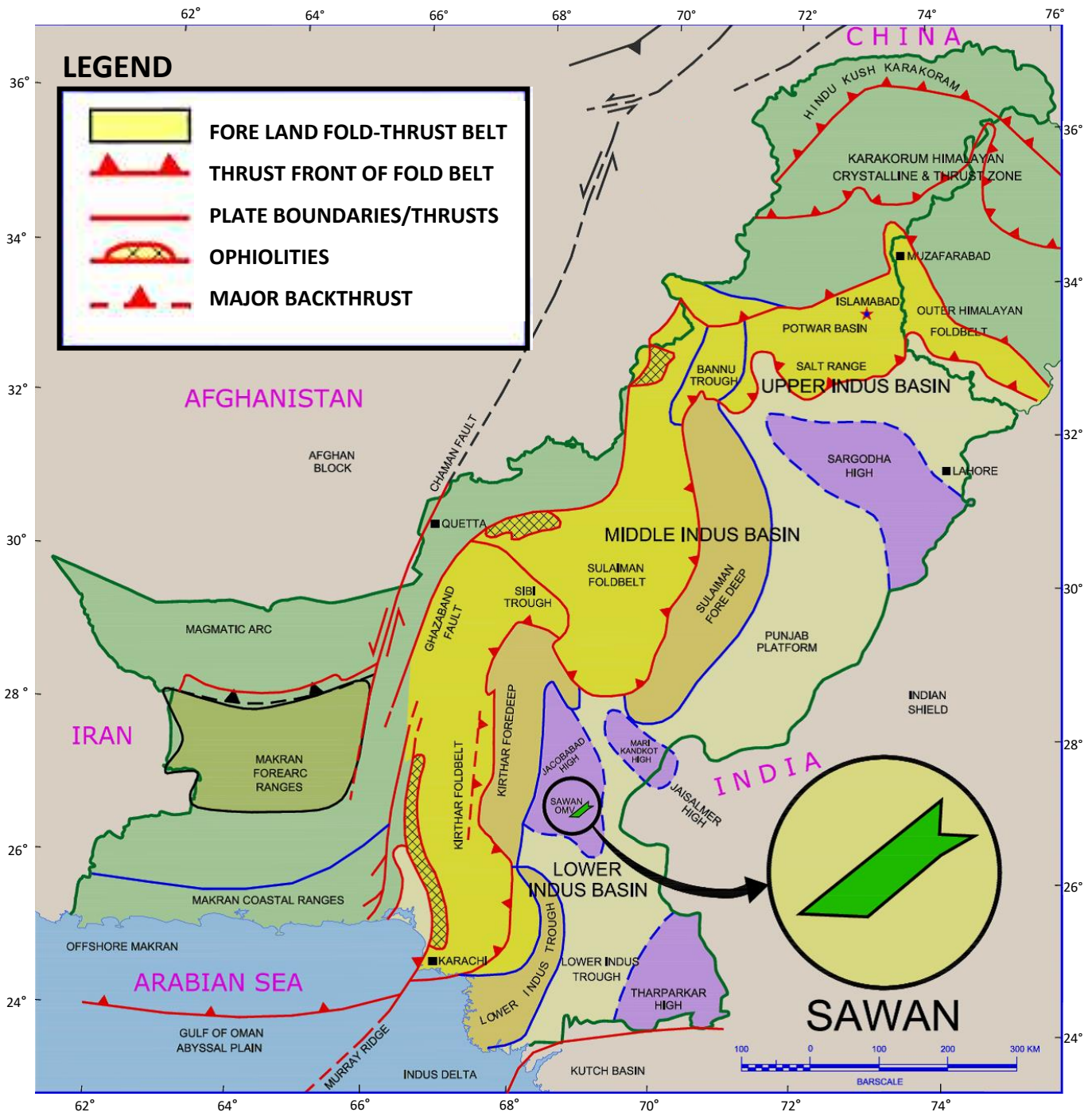
680 Zaigham, N.A., Mallick, K.A., 2000. Prospect of hydrocarbon associated with fossil-rift  
681 structures of the southern Indus basin, Pakistan. AAPG, Bull 84(11), 1833-1848.

682 Zhang, H., Brown, R.J., 2001. A review of AVO analysis, CREWES Research Report, Volume  
683 13, 337-378

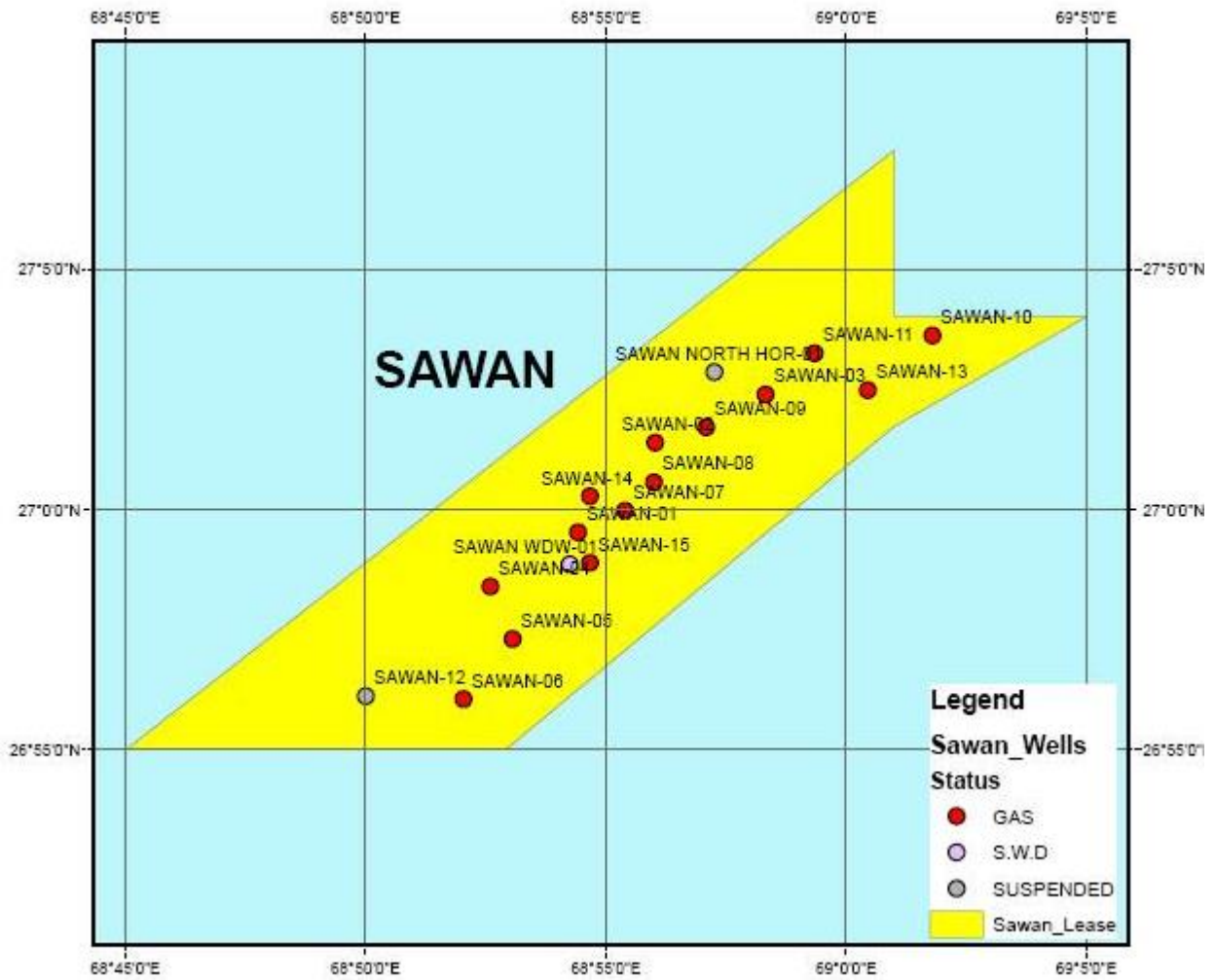
684 Zhu, Y., Xu, S., Payne, M., Martinez, A., Liu, E., Harris, C., Bandyopadhyay, K., 2012.  
685 Improved Rock-Physics Model for Shale Gas Reservoirs. SEG Technical Program Expanded  
686 Abstracts, 1-5.doi: 10.1190/segam2012-0927.1

687 Zoeppritz, K.E., 1919. On the reflection and propagation of seismic waves. Göttinger  
688 Nachrichten, 1(5), 66-84.

689



690  
 691 Figure 1a: Regional map showing the regional structural setting of Pakistan and the location of  
 692 multiple sedimentary basins in this country. The location of Sawan gas field is highlighted by  
 693 the black circle.



694

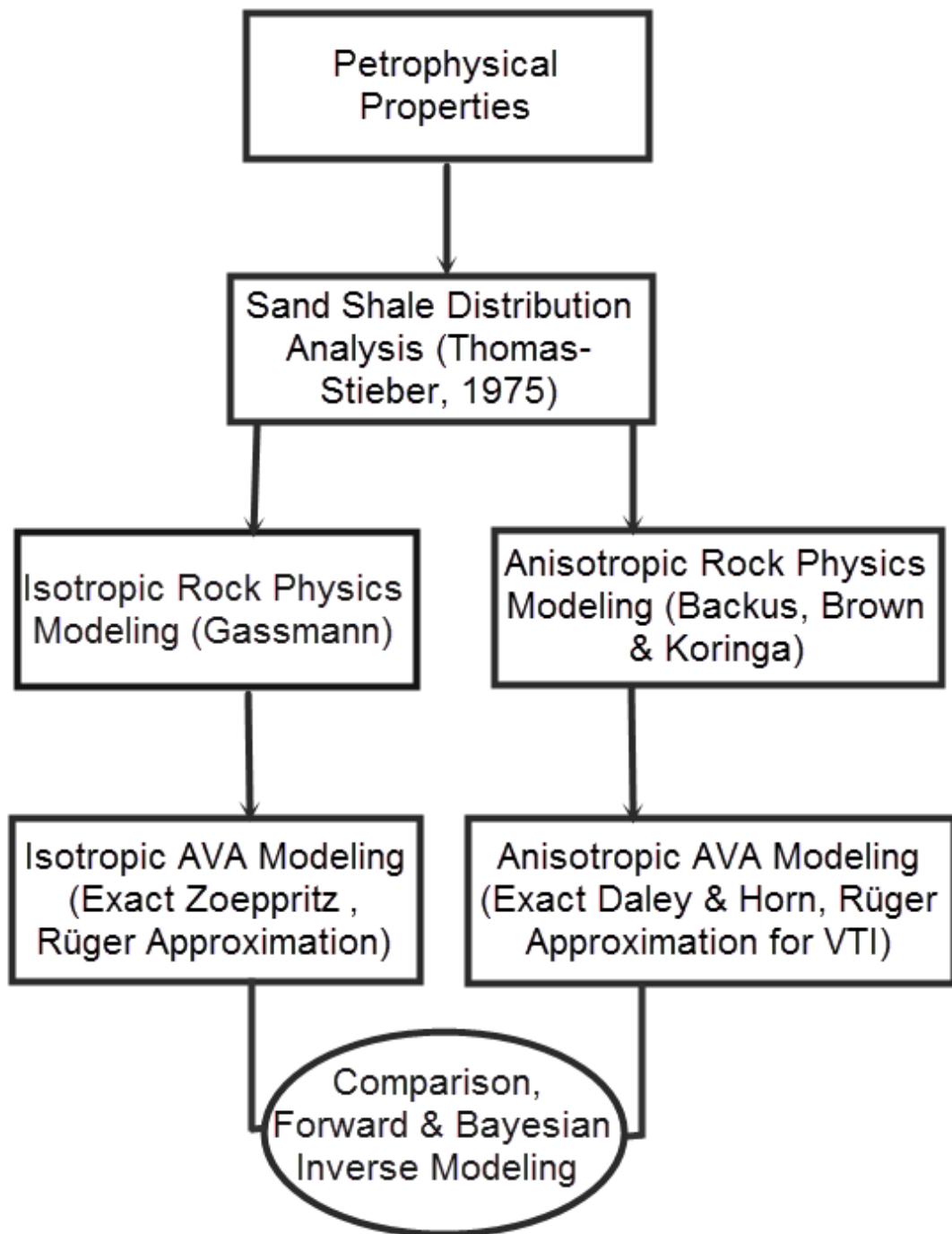
695 Figure-1b: Local map showing the boundaries of the Sawan gas field and the relative location  
 696 of exploration wells in the study area.

AGE	STRATIGRAPHY	LITHOLOGY	RESERVOIR POTENTIAL			OIL / GAS SHOWS	FIELDS		
			SOURCE	CAPROCK	RESERVOIR				
RECENT / PLEISTOCENE	ALLUVIUM / SIWALIKS								
E O C E N E	KIRTHAR FM.	DRAZINDA MB.			C				
		PIRKOH MB.				R			
		SIRKI MB.			C				
		HABIB RAHI MB.				R	*	Mari	
	LAKI FM.	GHAZIJ MB.			C				
		SUI MAIN LST. MB.				R	*	Kandhkot, Sui Qadirpur, Pirkoh	
PALEOCENE	DUNGHAN FM.			C		R	*	Zarghun	
	RANIKOT FM.			C		R	*	Pirkoh	
	PARH FM.								
UPPER CRETACEOUS	GORU FM.	UPPER GORU MB.							
		LOWER GORU MB.	SHALE INTERVAL		S	C			
			"D" INTERVAL				C		
			"C" INTERVAL		S	C	R	*	Sawan, Mari Latif
			"B" INTERVAL		S	C	R	*	Miano, Rehmat, Kadanwari
"A" INTERVAL				R	*				
LOWER CRETACEOUS	SEMBAR		S						
JURASSIC	CHILTAN								

697

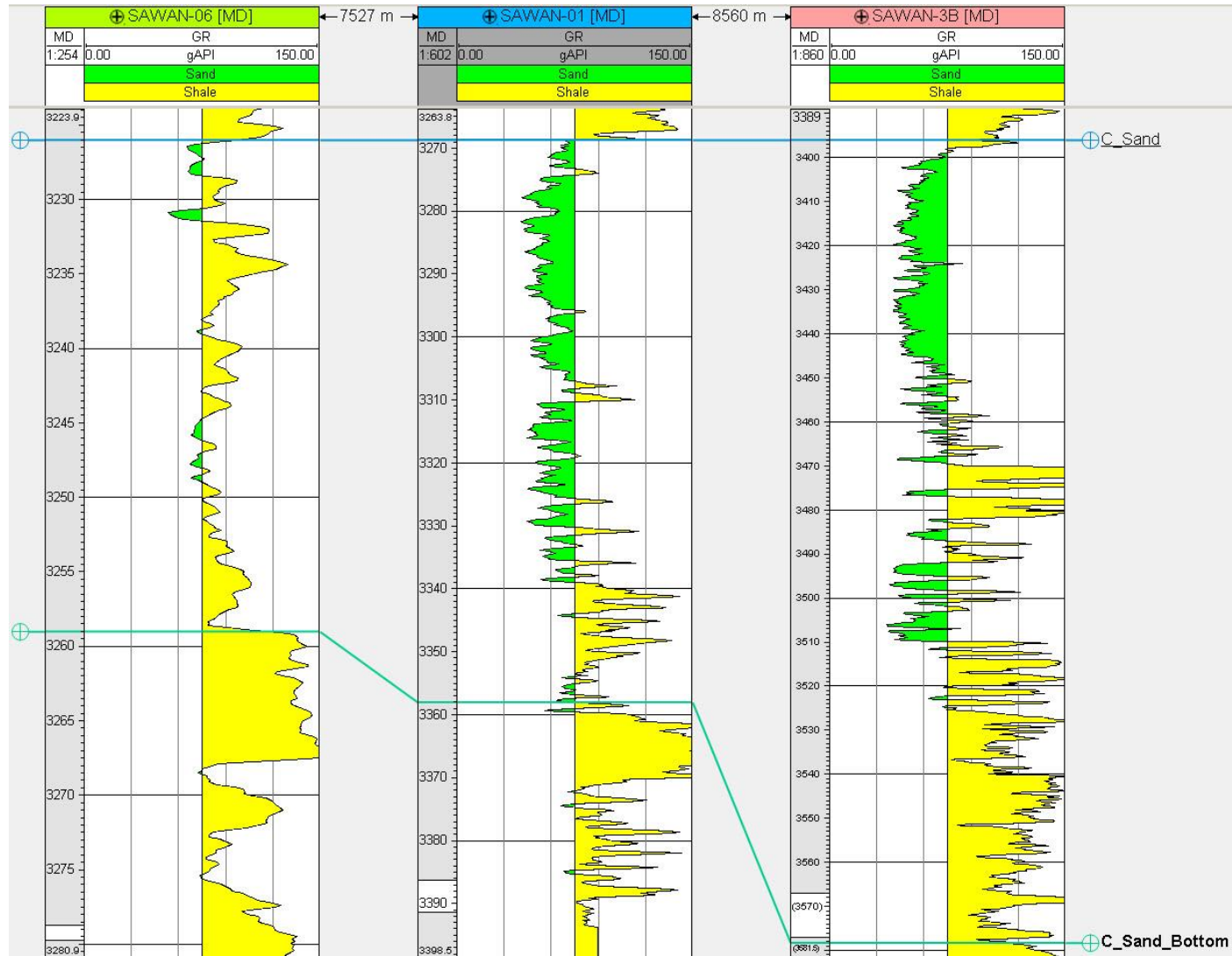
698 Figure 2: Generalised stratigraphy of the Sawan gas field highlighting the presence of multiple  
699 lithological units, including the Lower Goru C-sand interval and shaley intervals within and  
700 adjacent to these reservoir sands. This C-sand interval comprises the principal gas-producing  
701 reservoir of the Sawan field (Azeem et al., 2015).

702



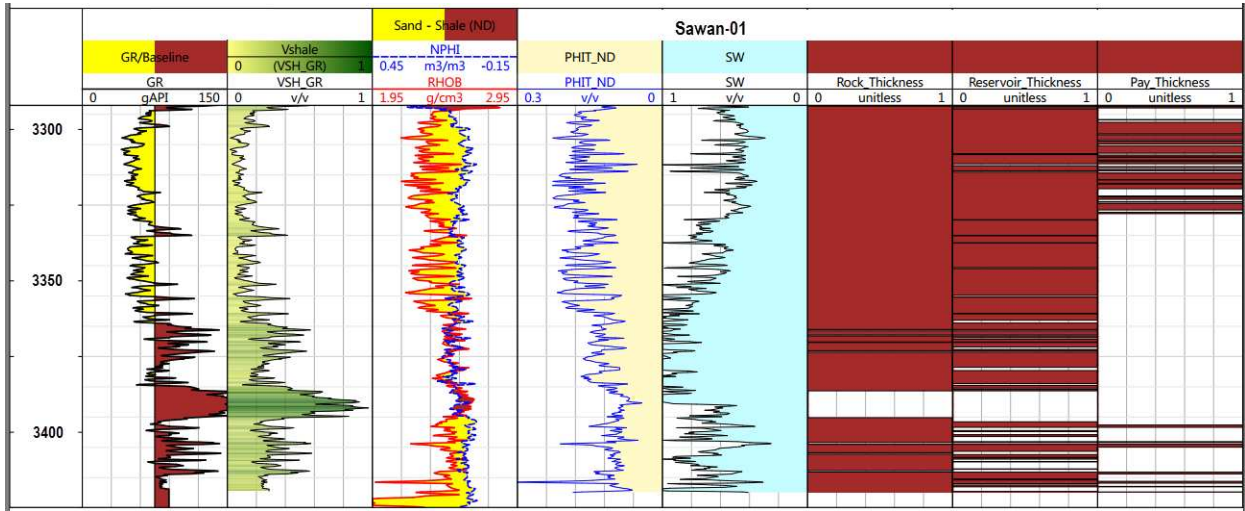
703  
704  
705  
706

Figure 3: Work Flow diagram showing the methodology adopted to compare isotropic and anisotropic AVA modelling.



707

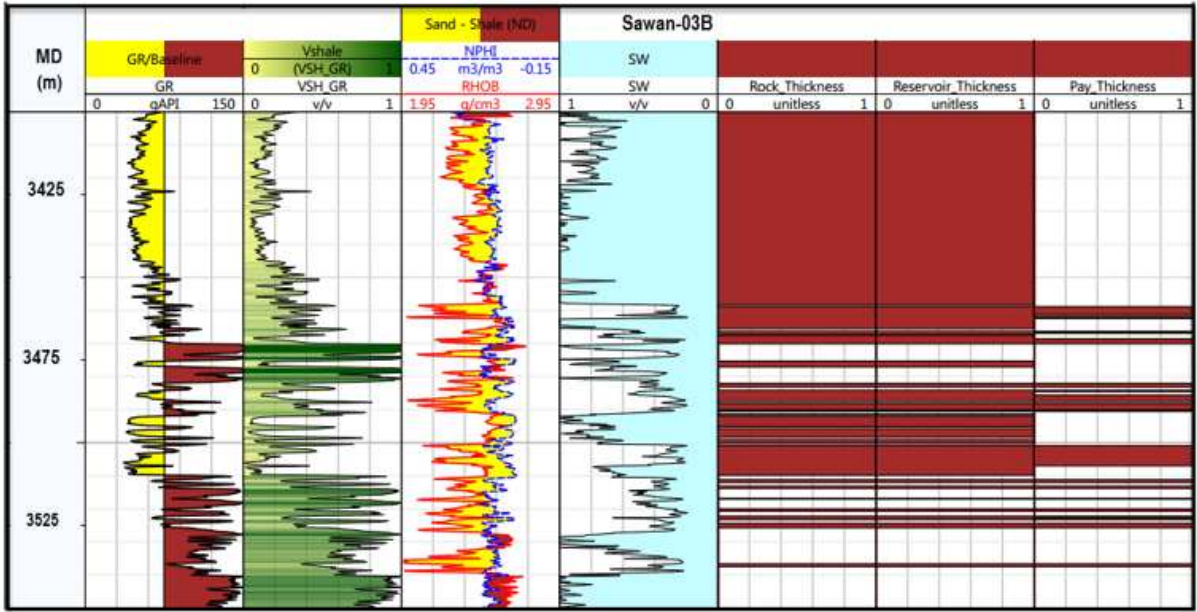
708 Figure 4 Well-log correlations for the Lower Goru C-sand and shale intervals in the three exploration wells used in AVA modelling.



709

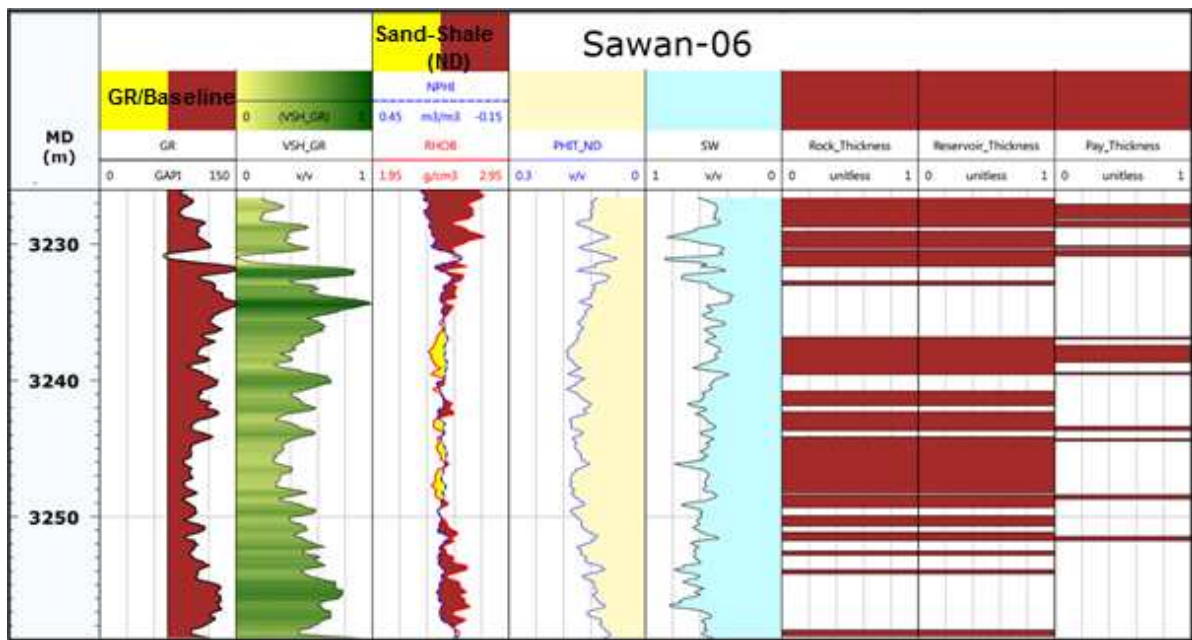
710 Figure 5: Results of petrophysical analyses for the estimation of reservoir properties of sand-  
 711 shale intervals in the Sawan-01 well.

712



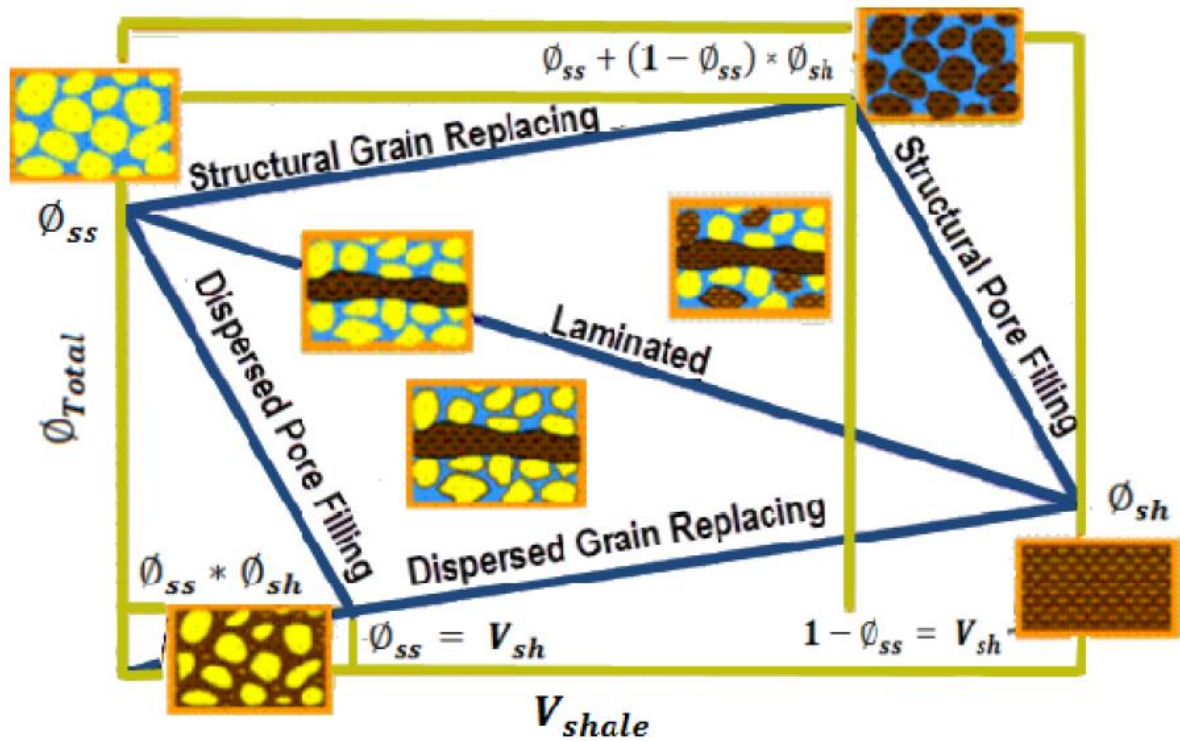
713

714 Figure 6: Results of petrophysical analyses for the estimation of reservoir properties of sand-  
 715 shale intervals in the Sawan-3B well.



716

717 Figure 7. Results of petrophysical analyses for the estimation of reservoir properties of sand-  
 718 shale intervals in the Sawan-06 well.

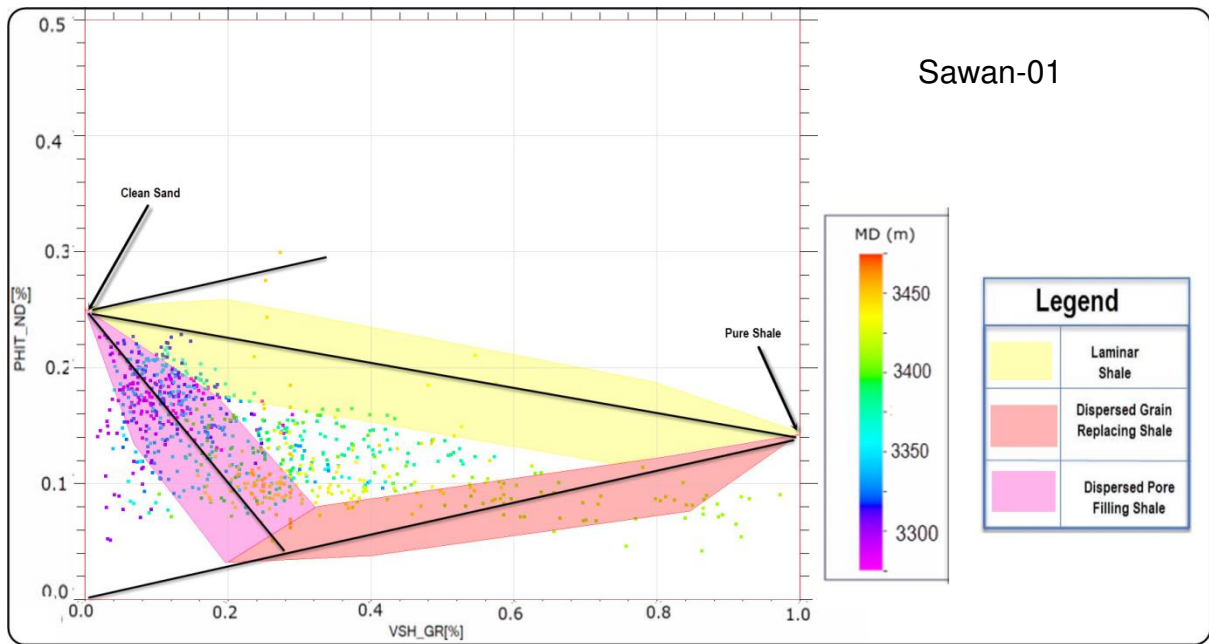


719

720 Figure 8: Shale distribution model proposed by Thomas and Strieber (1975) (figure modified  
 721 from Tyagi et al., 2009). In this diagram,  $V_{shale}$  is the volume of shale,  $\phi_{total}$  is the total  
 722 porosity,  $\phi_{max}$  is the maximum porosity, and  $\phi_{sh}$  is the porosity in shales.

723

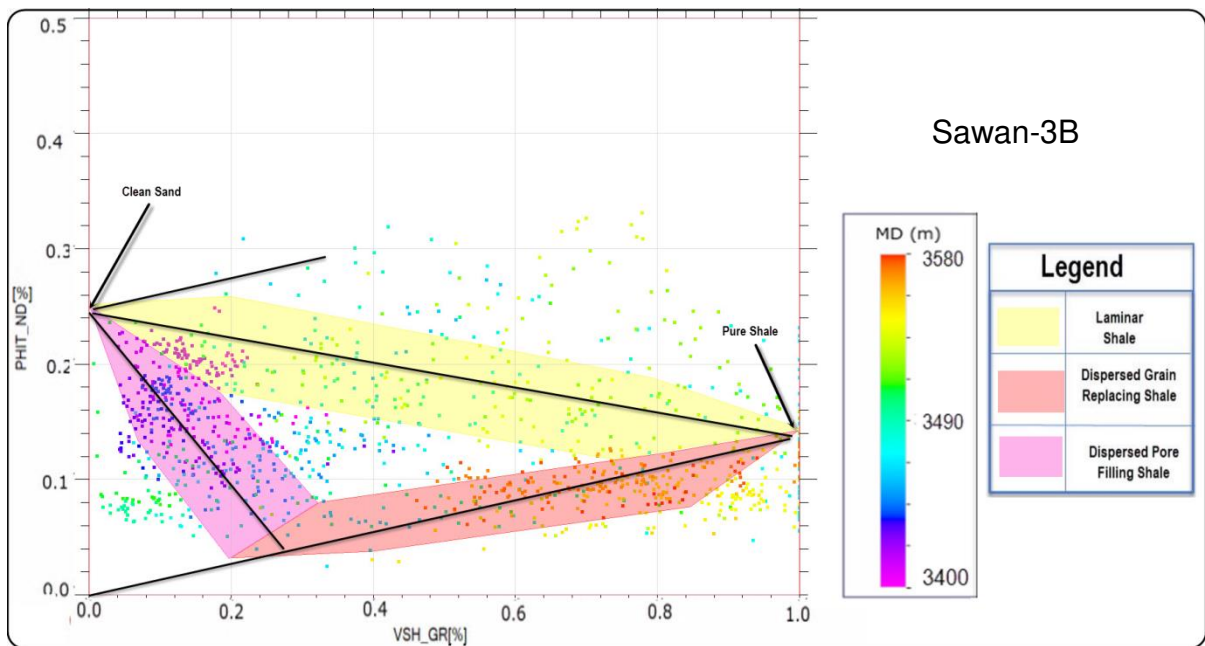
724



725

726 Figure 9: Cross-plots between volume of shale (X-axis) and total porosity (Y-axis). Based  
727 upon the position of data points, shale distribution was characterised within the C-sand  
728 reservoir in the Sawan-01 well.

729

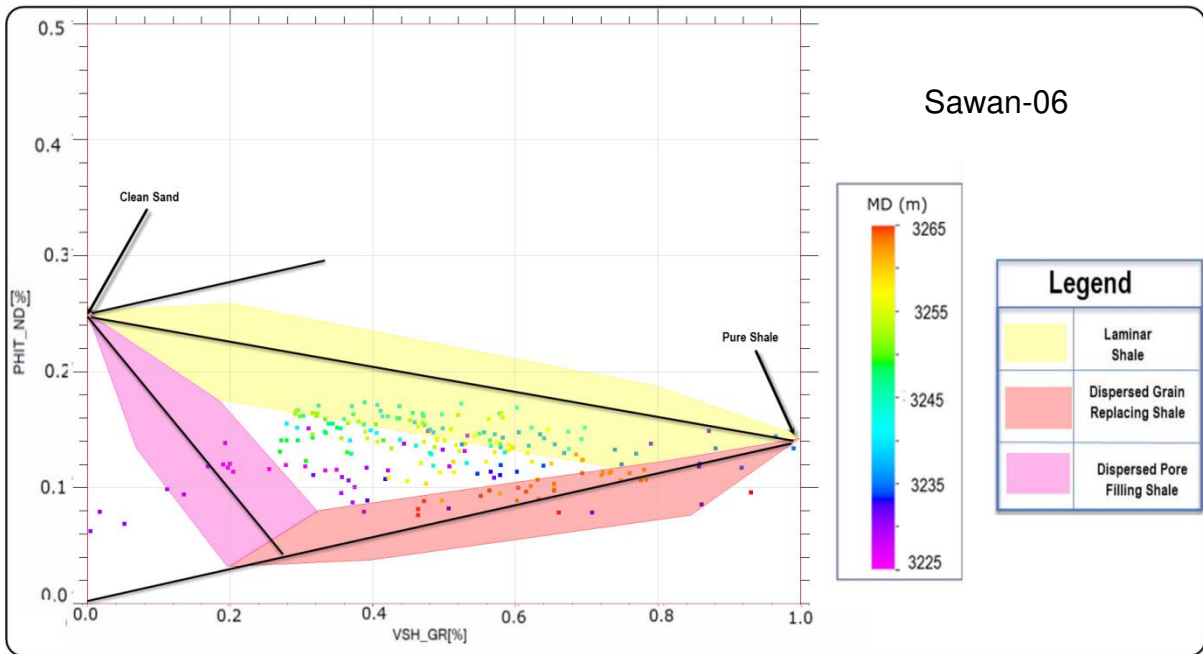


730

731 Figure 10: Cross-plots between volume of shale (X-axis) and total porosity (Y-axis). Based

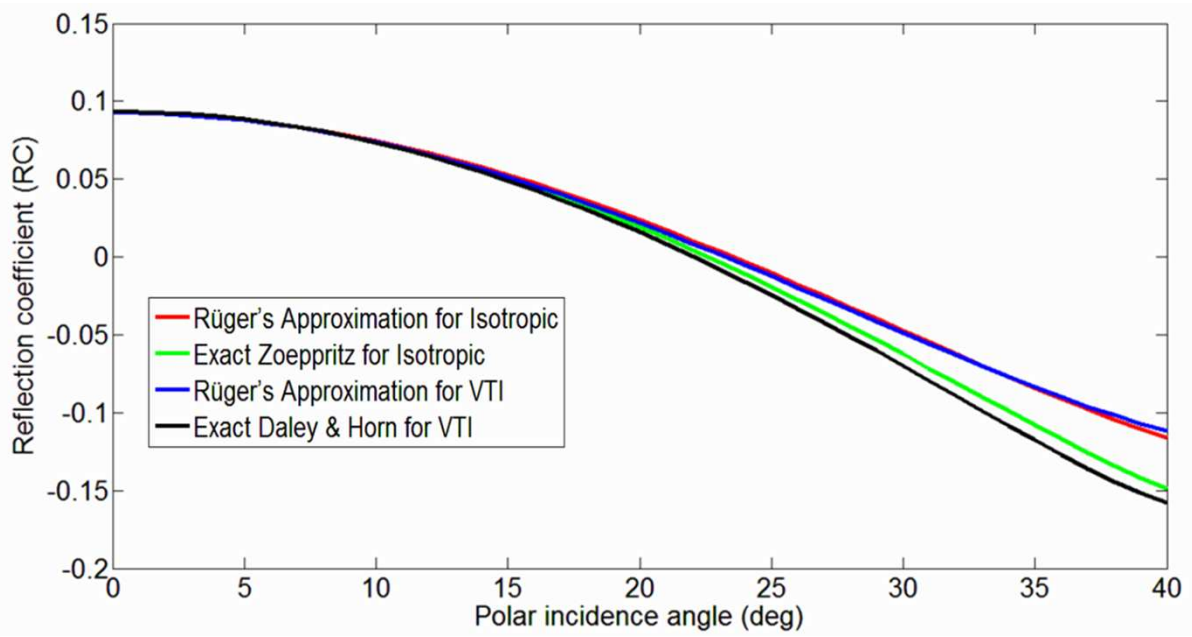
732 upon the position of data points, shale distribution was characterised within the C-sand

733 reservoir in the Sawan-3B well.



734

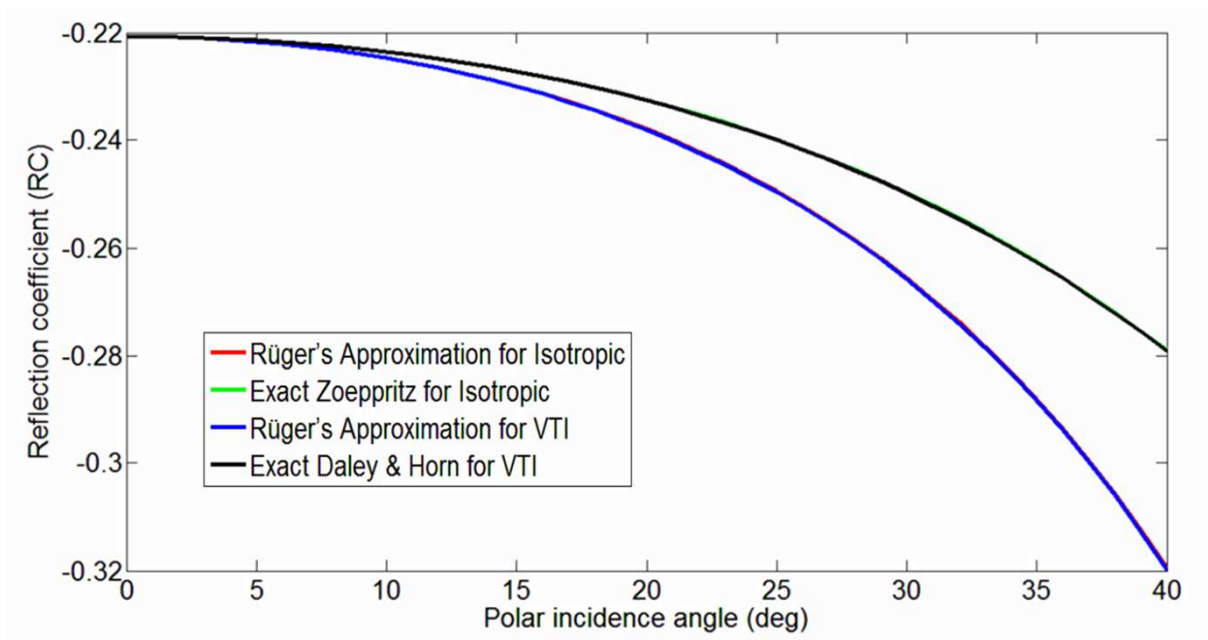
735 Figure 11: Cross-plots between volume of shale (X-axis) and total porosity (Y-axis). Based  
 736 upon the position of data points, shale distribution was characterised within the C-sand  
 737 reservoir in the Sawan-06 well.



738

739 Figure 12: Angle-dependent reflection coefficient data generated through the exact and  
 740 approximate solutions of PP-wave for isotropic and anisotropic (VTI) media at the top of C-  
 741 sand reservoir (Sawan-01 well).

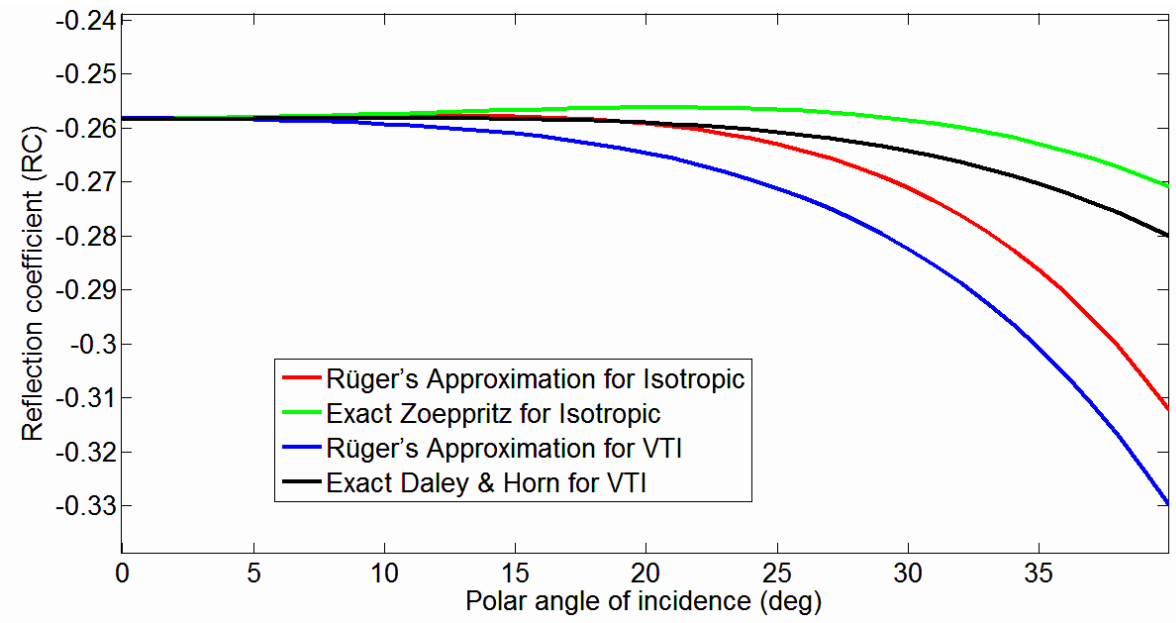
742



743

744 Figure 13: Angle-dependent reflection coefficient data generated through the exact and  
 745 approximate solutions of PP-wave for isotropic and anisotropic (VTI) media at the top of C-  
 746 sand reservoir (Sawan-3B well).

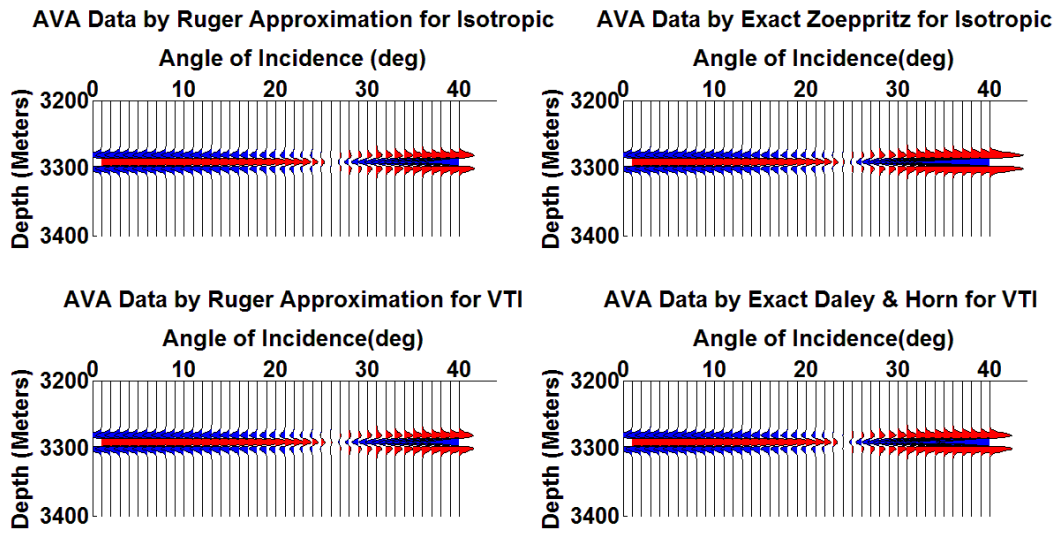
747



748

749 Figure 14: Angle-dependent reflection coefficient data generated through the exact and  
 750 approximate solutions of PP-wave for isotropic and anisotropic (VTI) media at the top of C-  
 751 sand reservoir (Sawan-06 well).

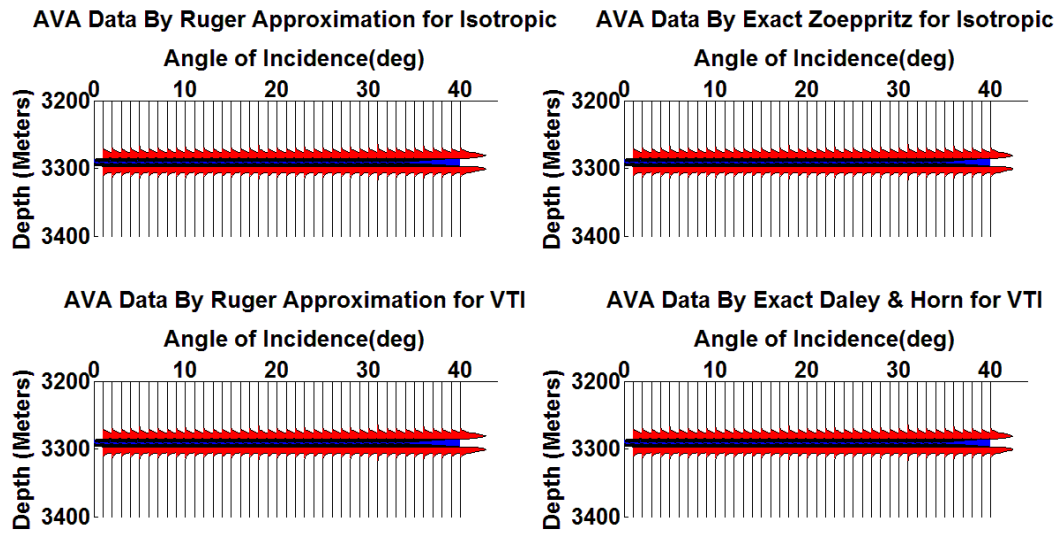
752



753

754 Figure 15: Seismic AVA response for the Lower Goru C-sand, Sawan-01 well.

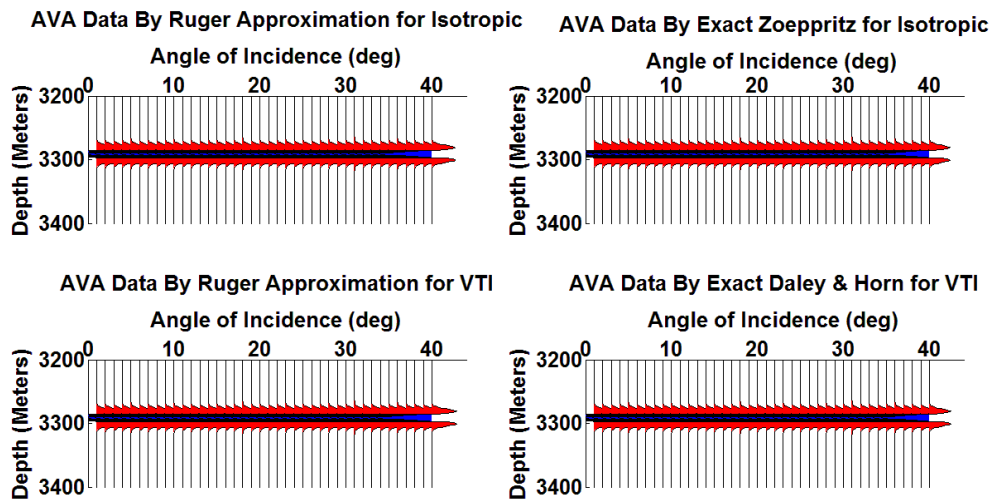
755



756

757 Figure 16: Seismic AVA response for the Lower Goru C-sand, Sawan-3B well.

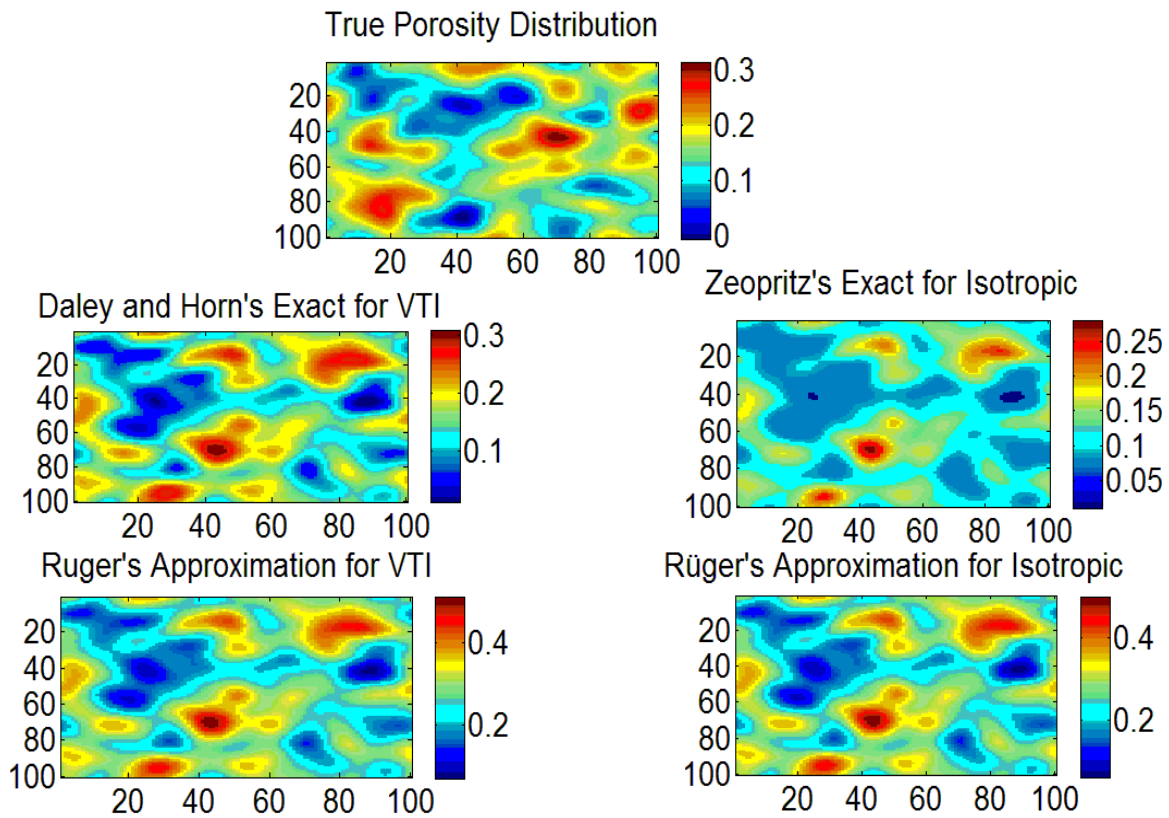
758



759

760 Figure 17: Seismic AVA response for the Lower Goru C-sand, Sawan-06 well.

761



762

763 Figure 18: Maps highlighting the inversion with 20% uncertainty for true porosity distribution  
 764 (top) generated via a correlated Gaussian field distribution throughout the reservoir interval at  
 765 100×100 grid blocks. These porosity plots were compiled via maximum a posteriori solution  
 766 under Bayesian settings utilising the rock physical properties of C-sand reservoir interval  
 767 (3268-3432 m) with exact and approximate solutions of PP-reflection coefficients for the  
 768 isotropic and anisotropic (VTI) cases. Inversion results show that Daley & Horn's (1977) exact  
 769 solution for VTI (left in 2<sup>nd</sup> row) returns porosity trends that are accurately aligned with the  
 770 true porosity distribution of the reservoir.

771

<b>Reservoir Properties</b>	<b>Sawan-01</b>	<b>Sawan-3B</b>	<b>Sawan-06</b>
Depth Range (m)	3268-3432	3398-3592	3227-3312
Gross Thickness (m)	164	184	85
Net Reservoir Thickness (m)	80	126	36
Net Pay Thickness (m)	24	58	20
Avg Porosity (%)	15	14	12
Avg Volume of Shale (%)	28	22	34
Average Water Saturation (%)	46	40	45

772 **Table 1:** Reservoir properties of the Sawan wells used in this study.

773

Cut-off	GR<=75 API	0.1<=NPHI<=0.45	Sw<=50%
Rock Thickness (m)	Yes	No	No
Net Reservoir Thickness (m)	Yes	Yes	No
Net Pay Thickness (m)	Yes	Yes	Yes

774 **Table 2:** Details of cut-off values used in the calculation of reservoir properties in Table 1.

775

Well	Formation	$V_p(\alpha)$	$V_s(\beta)$	Density( $\rho$ )	Porosity( $\phi$ )
Sawan-01	Sand	4165	4112	2.32	0.15
	Shale	2668	2170	2.67	0.08
	Overburden	2874.5	2367.5	2.54	
Sawan-3B	Sand	4251	2562	2.44	0.13
	Shale	4487	2628	2.60	0.10
	Overburden	4258	2547	2.62	
Sawan-06	Sand	4148.628	2579.0	2.51	0.13%
	Shale	4462.847	1741.0	2.61	0.085%
	Overburden	4322.960	2520.0	2.57	

776 **Table 3:** Mechanical properties of reservoir sand, intra-reservoir shale layers and overburden

777 used in the calculation of reflection coefficients.

778

<b>Material</b>	<b>Shear modulus (GPa)</b>	<b>Bulk modulus (GPa)</b>	<b>Density (g/cm<sup>3</sup>)</b>
Solid Mineral (Quartz)	44	37	2.65
Gas	0.0	0.025	0.065
Fluid (water/brine)	0.0	2.2	1.035

**Table 4:** Values of elastic moduli and densities for solid mineral and fluid used in our rock physics modelling.

780 **Appendix-A**

781 **Backus Averaging Approach**

782 The effective stiffness is anisotropic for a stratified medium composed of transversely  
 783 isotropic layers in the limit of long-wavelength, and represented by the Backus (1962) matrix  
 784 below (Mavko et al., 2009):

$$785 \begin{bmatrix} A & B & F & 0 & 0 & 0 \\ B & A & F & 0 & 0 & 0 \\ F & F & C & 0 & 0 & 0 \\ 0 & 0 & 0 & D & 0 & 0 \\ 0 & 0 & 0 & 0 & D & 0 \\ 0 & 0 & 0 & 0 & 0 & M \end{bmatrix}, \quad M = \frac{1}{2}(A - B), \quad (\text{A-I})$$

786 where  $A$ ,  $B$ ,  $C$ ,  $D$  and  $F$  are the five independent elastic constants

787 [i.e.,  $C_{11}$ ,  $C_{13}$ ,  $C_{33}$ ,  $C_{55}$  &  $C_{66}$ ]. In terms of P- and S-wave velocities ( $V_P$  and  $V_S$ ) and densities

788 ( $\rho$ ), the five independent elastic constants can be written as:

$$789 A = \left\langle 4\rho V_S^2 \left[ 1 - \frac{V_S^2}{V_P^2} \right] \right\rangle + \left\langle 1 - 2 \frac{V_S^2}{V_P^2} \right\rangle^2 \left\langle (\rho V_P^2)^{-1} \right\rangle^{-1}, \quad (\text{A-II})$$

$$790 B = \left\langle 2\rho V_S^2 \left[ 1 - \frac{2V_S^2}{V_P^2} \right] \right\rangle + \left\langle 1 - 2 \frac{V_S^2}{V_P^2} \right\rangle^2 \left\langle (\rho V_P^2)^{-1} \right\rangle^{-1}, \quad (\text{A-III})$$

$$791 C = \left\langle (\rho V_P^2)^{-1} \right\rangle^{-1}, \quad (\text{A-IV})$$

$$792 D = \left\langle (\rho V_S^2)^{-1} \right\rangle^{-1}, \quad (\text{A-V})$$

$$793 F = \left\langle 1 - 2 \frac{V_S^2}{V_P^2} \right\rangle^2 \left\langle (\rho V_P^2)^{-1} \right\rangle^{-1}, \quad (\text{A-VI})$$

794  $M = \langle \rho V_s^2 \rangle.$  (A-VII)

795 The brackets  $\langle \cdot \rangle$  indicate averages of the enclosed properties weighted by their volumetric  
796 proportions. Once the five independent constants are obtained, the Thomsen anisotropy  
797 parameters for VTI can be obtained using the relationships given by Thomsen (1986, 1995):

798  $\gamma = \frac{M-D}{2D},$  (A-VII)

799  $\varepsilon = \frac{A-C}{2C},$  (A-VIII)

800  $\delta = \frac{(F+D)^2 - (C-D)^2}{2C(C-D)}.$  (A-IX)

801 In order to calculate the effect of fluid saturation on the effective properties of a sand-shale  
802 layered medium, we have used the Gassmann (1951) equation for isotropic media, and the  
803 relationships of Brown and Korringa (1975) for anisotropic (VTI) media (Ali et al., 2011;  
804 Shahraini et al., 2011).

805

## 806 Appendix-B

### 807 1. Gassmann (1951) fluid substitution model for isotropic media

808 As the dry composite sand-shale medium was assumed as isotropic in this work, we used the  
809 low frequency Gassmann (1951) model (Equation B-I) applicable to well-connected porous  
810 media under isobaric conditions. We used this latter model in order to incorporate fluid  
811 effects into the effective mechanical properties calculated in our own models. Equation (B-I)  
812 defines a relationship between saturated bulk modulus, bulk modulus of the skeleton of the  
813 rock, bulk modulus of mineral comprising rock matrix, fluid bulk modulus and porosity. A  
814 typical form of the Gassmann (1951) equation is as follows:

815

$$816 \quad K_{sat} = K_{dry} + \left\{ \frac{\left( 1 - \left( \frac{K_{dry}}{K_{grain}} \right) \right)}{\left( \frac{\phi}{K_{fluid}} + \frac{1-\phi}{K_{grain}} \frac{K_{dry}}{K_{grain}^2} \right)} \right\}. \quad (B-I)$$

817 Here ' $K_{sat}$ ' is the saturated rock bulk modulus, ' $K_{dry}$ ' is the frame or dry bulk modulus,  
818 ' $K_{grain}$ ' is the grain bulk modulus, ' $K_{fluid}$ ' corresponds to the fluid bulk moduli, and ' $\phi$ ' is  
819 the porosity.

820

### 821 2. Brown and Korrington (1975) relations for fluid effects of an anisotropic medium

822 (VTI)

823

824 In order to calculate the effect of fluid saturation on the effective properties of a sand-shale  
825 interval, assuming it as VTI medium, we have used the anisotropic relations of Brown and  
826 Korrington (1975), which can be written in the symbolic or matrix notation as (Ali et al., 2011):

827

828 
$$\mathbf{S}^* = \mathbf{S}_d^* + \frac{((\mathbf{S}_d^* - \mathbf{S}_m) : (\mathbf{I}_2 \otimes \mathbf{I}_2) : (\mathbf{S}_d^* - \mathbf{S}_m))}{\varphi^0 (\mathbf{I}_2 : \mathbf{S}_m : \mathbf{I}_2 - 1/k_f) - \mathbf{I}_2 : (\mathbf{S}_d^* - \mathbf{S}_m) : \mathbf{I}_2} \quad (\text{B-II})$$

829 Here,  $\otimes$  denotes the dyadic product,  $\mathbf{S}_m$  is the compliance tensor of the solid mineral  
 830 component (properties of mineral quartz were used in the case of sand-shale model),  $\mathbf{S}_d^*$  is the  
 831 effective compliance tensor for the dry sand-shale medium, and  $\mathbf{S}^*$  is the effective compliance  
 832 tensor for the saturated sand-shale medium. In Equation (B-II),  $\varphi^0$  is the total porosity and  $\mathbf{I}_2$   
 833 is the (symmetric) identity matrix for second-rank tensors.

834 In the case of a composite porous medium that is partially saturated with oil, gas and water,  
 835  $K_f$  may be regarded as the bulk modulus of an effective fluid given by Wood - also known as  
 836 the Reuss average (Mavko et al., 2009):

837

838 
$$\frac{1}{K_f} = \frac{S_w}{K_w} + \frac{S_o}{K_o} + \frac{S_g}{K_g}, \quad (\text{B-III})$$

839 where

840

841 
$$S_w + S_o + S_g = 1. \quad (\text{B-IV})$$

842 Here,  $S_w$ ,  $S_o$  and  $S_g$  represent the saturation for water, oil and gas, and  $K_w$ ,  $K_o$  and  $K_g$   
 843 represent the bulk modulus for water, oil and gas.